Title

Diffusion Breast MRI: Current Standard and Emerging Techniques

Authors

Mendez, Ashley M
Fang, Lauren K
Meriwether, Claire H
et al.

Publication Date

2022

DOI

10.3389/fonc.2022.844790

Peer reviewed

frontiers | Frontiers in Oncology

REVIEW
published: 08 July 2022
doi: 10.3389/fonc.2022.844790

Diffusion Breast MRI: Current Standard and Emerging Techniques

Ashley M. Mendez[1], *Lauren K. Fang*[1], *Claire H. Meriwether*[1], *Summer J. Batasin*[1], *Stéphane Loubrie*[1], *Ana E. Rodríguez-Soto*[1] *and Rebecca A. Rakow-Penner*[1,2*]

[1] Department of Radiology, University of California San Diego, La Jolla, CA, United States, [2] Department of Bioengineering, University of California San Diego, La Jolla, CA, United States

The role of diffusion weighted imaging (DWI) as a biomarker has been the subject of active investigation in the field of breast radiology. By quantifying the random motion of water within a voxel of tissue, DWI provides indirect metrics that reveal cellularity and architectural features. Studies show that data obtained from DWI may provide information related to the characterization, prognosis, and treatment response of breast cancer. The incorporation of DWI in breast imaging demonstrates its potential to serve as a non-invasive tool to help guide diagnosis and treatment. In this review, current technical literature of diffusion-weighted breast imaging will be discussed, in addition to clinical applications, advanced techniques, and emerging use in the field of radiomics.

Keywords: imaging biomarker, breast cancer, diffusion tensor (DT) MRI, non-gaussian diffusion, restriction spectrum imaging, diffusion weighted (DW) breast MRI, diagnostic breast imaging, radiomics

OPEN ACCESS

Edited by:
Samata Kakkad,
Merck, United States

Reviewed by:
Hadassa Degani,
Weizmann Institute of Science, Israel
Rita G. Nunes,
Universidade de Lisboa, Portugal

***Correspondence:**
Rebecca A. Rakow-Penner
rrakowpenner@health.ucsd.edu

Specialty section:
This article was submitted to Breast Cancer, a section of the journal Frontiers in Oncology

Received: *28 December 2021*
Accepted: *11 May 2022*
Published: *08 July 2022*

Citation:
Mendez AM, Fang LK, Meriwether CH, Batasin SJ, Loubrie S, Rodríguez-Soto AE and Rakow-Penner RA (2022) Diffusion Breast MRI: Current Standard and Emerging Techniques. Front. Oncol. 12:844790. doi: 10.3389/fonc.2022.844790

INTRODUCTION

The history of the role of magnetic resonance imaging (MRI) in visualizing breast cancer dates back to the 1980s, when it was discovered that breast malignancies enhanced significantly compared to normal breast tissue with the use of gadolinium contrast-enhanced MRI (1–3). In the decades since then, an abundance of evidence has emerged supporting the use of dynamic contrast enhanced (DCE)-MRI in the breast, with applications ranging from high risk screening and lesion characterization, to preoperative staging and breast cancer surveillance (1). At present, DCE protocols have been accepted as the standard technique in the MRI evaluation of breast cancer by the American College of Radiology (ACR) (4). While DCE-MRI demonstrates high sensitivity in the detection of malignancy, it requires the administration of intravenous contrast, which is invasive, poses a potential risk for unknown long term gadolinium-related side effects, and is contraindicated in certain patient populations, such as pregnant women.

Diffusion-weighted imaging (DWI) has emerged as both a complementary and potentially alternative technique to evaluate the breast. By measuring the diffusion of water molecules, quantified as the apparent diffusion coefficient (ADC), DWI provides insight into the micro-structural features of tissues (**Figure 1**). *In vivo*, the diffusion of water molecules can be categorized into three principal physical modes: free, hindered, and restricted (including partially restricted) (5–8). Free diffusion in tissues represents the random (Brownian), unhindered motion of water molecules, following a Gaussian distribution (5). Hindered diffusion represents the impeded motion of water molecules secondary to extracellular obstacles, such as high tumor cellularity (5). Restricted diffusion in tissues represents the inhibited motion of water molecules secondary to intracellular obstacles, such

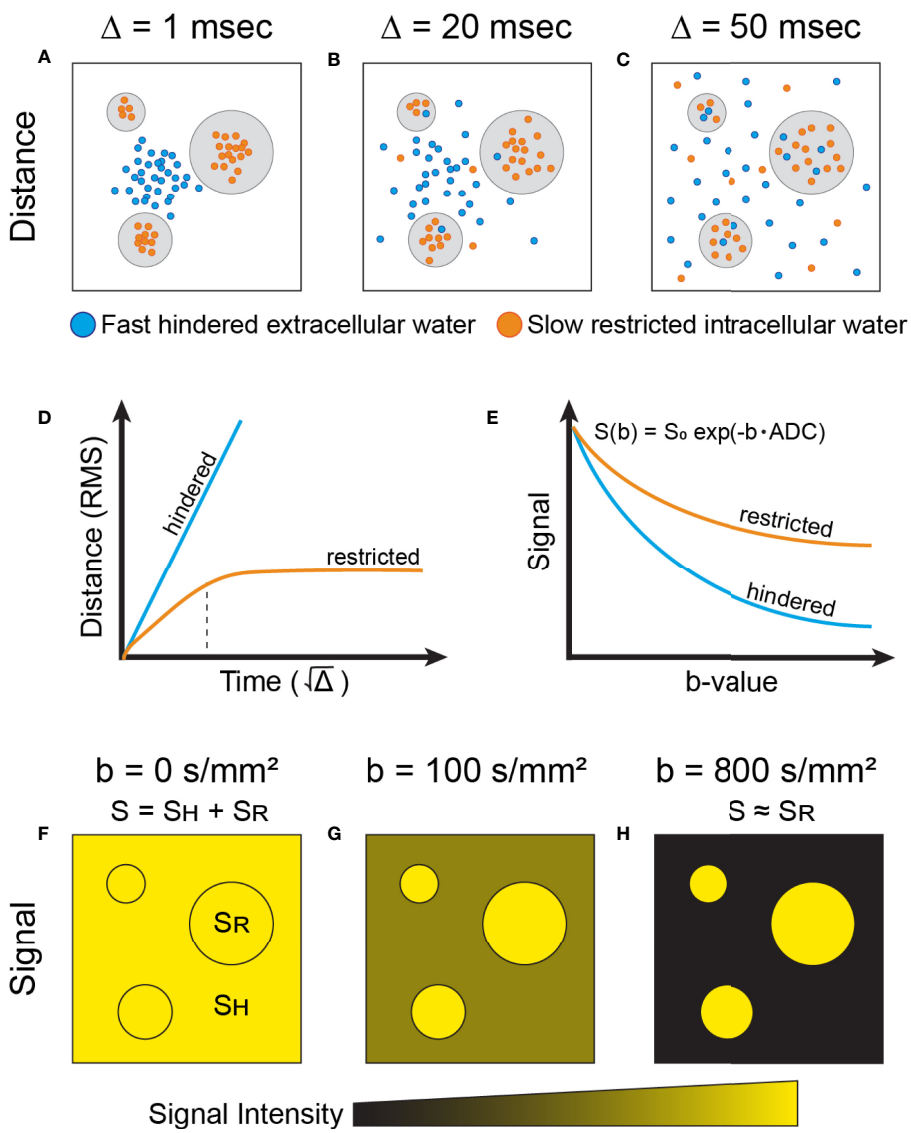

FIGURE 1 | Simplified physical basis of advanced diffusion imaging. Water molecules moving at two different speeds are shown: fast-moving (free and hindered) which exist in extracellular space (blue), and slow-moving (restricted) molecules that are trapped intracellularly by the plasma membrane (orange). Note that exchange between the extra- and intracellular compartments also exists, dictated by membrane permeability. The schematic shows the dispersion of these water molecular diffusing across cellular compartments, at different timescales (Δ) of **(A)** 1msec, **(B)** 20 msec, and **(C)** 50 msec. **(D)** The root mean square (RMS) distance of water molecules experiencing hindered diffusion is linear with respect to the $\sqrt{\Delta}$ (i.e. Gaussian diffusion, blue). In contrast, slow-moving water molecules in the intracellular compartment display Gaussian diffusion behavior (linear) at very short timescales (panel **D**, orange), dictated by the compartment's intrinsic diffusivity (5). At intermediary timescales, molecules reach the plasma membrane boundary that restricts movement, indicated by the dotted black vertical line. Past this, the net squared displacement becomes sublinear with time and is dependent on the dimensions of the compartment. To note, at very long diffusion timescales (Δ>1s), restricted water diffusion becomes principally governed by the exchange rate between the intra- and extracellular compartments (5). **(E)** In DW-MRI, the measured signal (S) decays exponentially (in the case of Gaussian diffusion) with respect to b-value due to loss of spin coherence caused by dispersion of water molecules. Thus, the signal decay from water molecules experiencing hindered diffusion (blue) is faster than from water molecules experiencing restricted diffusion (orange). The measured diffusion signal at different b-value weighting **(F–H)** reflects the relative dephasing of water molecules in different tissue compartments. At short timescales **(A, F),** the measured signal, S, contains combined information from both hindered (S_H) and restricted (S_R) water signal. At progressively longer timescales **(B, C, G, H)**, signal from hindered water dissipates more quickly than that from restricted water due to increased motion along the diffusion gradient axis, and the measured signal begins to arise predominantly from the restricted water signal (5). As shown in panel **(E)**, restricted water will retain more signal at higher b-values than hindered water and, correspondingly, have a lower ADC than hindered water.

as a cell-membranes, and follows a non-Gaussian distribution (5). To note, whereas hindered extracellular diffusion is independent of diffusion time (dictated by the time delay between diffusion sensitizing gradients), restricted diffusion is dependent on the diffusion time, membrane permeability, and the size of the restricting cellular compartments (5).

The degree of diffusion weighting in standard DWI is measured by the b-value (s/mm^2), a parameter determined by multiple experimental variables including the gradient strength, gradient duration, and time delay between diffusion sensitizing gradients (5, 9). The ADC value, defined as the average area occupied by a water molecule per unit time (mm^2/s), can be estimated from the signal measured from two different acquisitions, one with diffusion weighting (non-zero b-value) and one without (b=0 s/mm^2), according to the formula

$$S_D = S_0 e^{-b \cdot ADC} \quad [1]$$

where S_D is the diffusion weighted signal intensity, S_0 is the signal intensity without diffusion weighting and b is the diffusion sensitization factor in s/mm^2 (10). Equation 1 assumes a single tissue compartment and hence mono-exponential decay (Gaussian diffusion), which is an approximation for a given tissue at a specified b-value range. At typical clinically used diffusion times (e.g. 50-100 ms), tissues with more hindered and restricted diffusion will often yield lower ADC values (3). Therefore, ADC may serve as a surrogate for tissue cellularity and thus an imaging biomarker for breast cancer (**Figure 2**). This review article will focus on standard and emerging DWI techniques and their application to breast imaging.

CLINICAL APPLICATIONS

Screening

The current ACR guidelines recommend screening mammography starting at the age of 40 for women with average risk of breast cancer. For women with higher than average risk—defined as having a ≥20% lifetime risk, genetic predisposition for breast cancer, or history of radiotherapy to the chest—or a personal history of breast cancer and dense breast tissue, annual contrast-enhanced breast MRI is recommended (11). At present, DCE-MRI is the standard of care, but the role of DWI in screening is being explored.

Superior performance of DWI in the evaluation of mammographically occult and non-palpable breast cancers, particularly in women with dense breasts, compared to mammography alone has been reported (12, 13). Greater visibility of mammographically occult breast cancer on DWI compared to ultrasound was shown by Amornsiripanitch et al. (14). Compared to DCE-MRI, Pinker et al. showed that current DWI as a stand-alone tool demonstrates inferior sensitivity and diagnostic performance (15). However, the combination of DCE and DWI increased specificity and maximized diagnostic accuracy (15). Therefore, although currently not part of the BI-RADS lexicon, the inclusion of DWI in the MRI evaluation of breast cancer is encouraged by the European Society of Breast Imaging (16).

Despite evidence showing the high diagnostic accuracy of breast MRI, the financial cost and long acquisition times limit widespread implementation as a screening method in women of average risk (17). These limitations inspired the development of abbreviated breast MRI (abMRI) protocols (17). A meta-analysis of five studies found that abMRI protocols, which included first contrast-enhanced acquisition subtracted (FAST) sequences, demonstrated comparable sensitivity and specificity to standard MRI protocols in the setting of breast cancer screening (17).

Unenhanced abbreviated protocols with DWI sequences have been developed to address the drawbacks of DCE imaging, including cost, invasiveness, and safety concerns regarding the potential long-term effects of gadolinium. Studies showed comparable specificity of unenhanced abbreviated protocols that include DWI compared to either abbreviated contrast enhanced protocols or standard full DCE-MRI acquisitions (12, 13, 18–22). However, several of these studies evaluated cohorts with known malignancy (12, 13, 18), and many found that abbreviated DWI had lower sensitivity than DCE-MRI (12, 13, 18, 19, 21). Unenhanced abbreviated protocols are partly limited by decreased lesion conspicuity and lower interreader agreement (18, 19, 21, 22). Overall, results suggest that an unenhanced abbreviated protocol can maintain high diagnostic performance and represent a potential

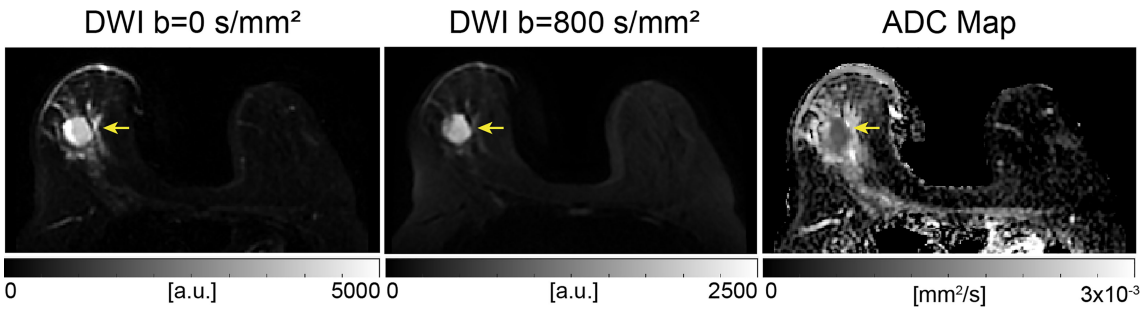

FIGURE 2 | Example of conventional breast DWI at 3T, shown at b-values 0 and 800 s/mm^2 and corresponding ADC map in a 49-year-old patient The lesion, indicated by the yellow arrow, has increased signal on b=800 s/mm^2 images and displays lower ADC values compared to surrounding tissue, indicating a finding suspicious for malignancy. This lesion was found to be an invasive ductal carcinoma from pathology.

time- and cost-effective adjunct to conventional screening protocols.

Lesion Detection and Characterization

Among the available breast imaging modalities, DCE-MRI has been established as the most sensitive in the detection of malignancy (23). Shared imaging features between benign and malignant lesions, however, limit specificity (23). The addition of DWI to DCE-MRI may offer a way of increasing diagnostic accuracy through improved specificity (24). A meta-analysis of 14 studies showed a pooled sensitivity and specificity of 91.6% and 85.5% for DCE-MRI with DWI, which was superior to DWI (86% and 75.6%) and DCE-MRI (93.2% and 71.1%) alone (25). These findings agree with other studies suggesting improved lesion characterization with multiparametric MRI (26–28). For example, a study by Pinker et al. evaluated the feasibility and diagnostic accuracy of multiparametric MRI (DCE imaging and DWI) at 7T and also found increased specificity compared to DCE-imaging alone, suggesting the addition of DWI as well as high resolution imaging may contribute to improved diagnostic accuracy (26). The added specificity from DWI holds potential to lower the false positive rate and decrease the number of unnecessary breast biopsies without missing malignancies (28).

Numerous studies have shown that DWI can be used to differentiate malignant from benign breast lesions, owing to the significantly hindered and restricted diffusion in breast cancers. A recent meta-analysis by Baxter et al. included 65 studies that evaluated the diagnostic performance of DWI and found a pooled sensitivity, specificity, and AUC of 89%, 82%, and 0.92 (29), respectively, which is comparable to results from multiple additional meta-analyses (30–32). Subgroup analysis showed that diagnostic performance was not significantly associated with the number or choice of b-values, field strength, or method of region of interest (ROI) segmentation (29).

Despite the comparable diagnostic performance of ADC across studies, threshold values varied. Small sample sizes with various proportions of lesion subtypes, differing field strengths, and selection of b-values have been suggested to contribute to this discrepancy. A recently published meta-analysis by Surov et al. aimed to provide clinically relevant information regarding use of ADC values in the differentiation of malignant and benign breast lesions (33). This analysis included 123 studies from across the world and a total of 13,847 breast lesions. The reported pooled mean ADC values for malignant versus benign breast lesions were 1.03×10^{-3} mm^2/s, 95% CI (1.01–1.05 $\times 10^{-3}$ mm^2/s) and 1.50×10^{-3} mm^2/s, 95% CI (1.45–1.55 $\times 10^{-3}$ mm^2/s), respectively (33). This study found that all benign lesions had ADC values above 1.0×10^{-3} mm^2/s, independent of field strength, choice of b-values, and ROI delineation technique (33). However, the study also demonstrated considerable overlap of malignant and benign lesions in the ADC range between 1 and 2×10^{-3} mm^2/s, which limits the clinical use of the proposed threshold value (33).

Diffusion-weighted imaging has also demonstrated potential in differentiating between invasive ductal carcinoma (IDC) and ductal carcinoma *in situ* (DCIS) (34–36). A meta-analysis of 15 studies showed a significantly higher ADC value in DCIS (0.92-1.56 $\times 10^{-3}$ mm^2/s) compared to IDC (0.89-1.31 $\times 10^{-3}$ mm^2/s) lesions, highlighting the microstructural differences between the two pathologies, potentially providing a noninvasive means of lesion characterization (34). Subgroup analysis stratified by ethnicity found lower ADC values in IDC compared to DCIS in the Asian population but not in Caucasians. Smaller sample size of Caucasian patients in this study (293 versus 858 Asians) may contribute to the differing results, as well as genetic and environmental differences (34).

Prognostic Factors

Prognostic factors for breast cancer are used to predict survival, guide treatments, and stratify patients into clinical trials. While some of these factors, such as stage or tumor size, can be provided by imaging, several others rely on pathologic diagnosis. The use of DWI has been explored as a potential non-invasive method of predicting prognostic factors. The driving hypothesis behind these studies is that malignant lesions demonstrate high proliferation, which causes the ADC values of tissues to decrease as a result of increased cellularity (37). Tumors with increased angiogenesis are suggested to display relatively higher ADC values from increased vascular permeability and increased extracellular fluid, although this hypothesis has not yet been validated (37). Several studies have evaluated the association of ADC values and prognostic factors in breast cancer, including tumor subtype, lymph node metastases, hormone receptor expression, and histologic grade, among others.

Lymph Node Metastasis

The identification of lymph node metastases is necessary for accurate staging of breast cancer, which in turn affects treatment planning and prognosis (38, 39). Tissue sampling remains the gold standard but is invasive and prone to sampling error (39). As a surrogate for underlying cellularity, DWI may provide a noninvasive way of evaluating the axilla. A meta-analysis of 10 studies and 2305 lymph nodes showed a significantly lower ADC for metastatic lymph nodes (benign: 0.75-1.77 $\times 10^{-3}$ mm^2/s vs. metastatic: 0.69-1.37 $\times 10^{-3}$ mm^2/s), with a pooled sensitivity and specificity of 89% and 83%, respectively (39), similar to results of a few other studies (40–42). A handful of studies, however, including a large multicenter analysis, found no correlation between ADC values and lymph node involvement (43–46).

Hormone Receptor Expression

The correlation between ADC and hormone receptor expression has also been explored, with varied results. A meta-analysis of 6 studies showed a negative correlation between ADC values and estrogen receptor (ER) and progesterone receptor (PR) expression (47), which is consistent with the results of a few additional studies (37, 44, 48). Other groups, however, found no association with ER or PR expression (40, 45, 49, 50). A positive correlation between ADC values and human epidermal growth factor receptor 2 (HER2) expression was shown by a few groups (40, 41, 45, 48, 51), whereas others found no association (43, 44, 46, 50, 52, 53). Conflicting results were also reported regarding histologic grade, with some studies demonstrating decreased ADC values with increasing grade (41, 42, 53, 54) and others

not finding a significant association (40, 52, 55, 56). Most studies found no significant association between ADC values and tumor size (42, 44, 46, 52, 53). Multiple factors may contribute to conflicting results, including differences in study design, technical parameters, and tumor types evaluated.

Histopathologic Subtype

The recommended treatment for breast cancer is highly dependent on biological subtype. For example, in terms of systemic treatment, Luminal A breast cancers generally only receive endocrine therapy, whereas the addition of cytotoxic therapy is indicated for most patients with Luminal B and triple negative breast cancer (57). Immunohistochemistry remains the gold standard for subtype classification but is costly and invasive. Multiple groups have investigated the potential for DWI to predict molecular subtype. A meta-analysis by Meyer et al. compared the ADC values between breast cancer subtypes and included 28 studies comprising 2990 lesions, of which 28.9% were classified as Luminal A, 30.1% Luminal B, 20% HER2 enriched, and 21% triple negative (58). Pooled data showed mean ADC values of 0.99×10^{-3} mm^2/s (95% CI 0.94–1.04×10^{-3} mm^2/s), 0.97×10^{-3} mm^2/s (95% CI 0.89–1.05×10^{-3} mm^2/s), 1.02×10^{-3} mm^2/s (95% CI 0.95–1.08×10^{-3} mm^2/s), and 0.99×10^{-3} mm^2/s (95% CI 0.91–1.07×10^{-3} mm^2/s) for these four subtypes, respectively (58). The large overlap in ADC values between subtypes is consistent with the results from a multicenter analysis by Surov et al., which found mean ADC values of $1.01 \pm 0.22 \times 10^{-3}$ mm^2/s, $0.95 \pm 0.23 \times 10^{-3}$ mm^2/s, $1.04 \pm 0.23 \times 10^{-3}$ mm^2/s, and $0.95 \pm 0.17 \times 10^{-3}$ mm^2/s for the four subtypes, respectively, suggesting that ADC values may not be a useful predictor of molecular subtype (43).

The proliferation index, Ki-67, is a component of the subtype classification differentiating Luminal A from Luminal B breast cancer, and therefore directly affects treatment strategy. A meta-analysis by Surov et al. found a weak negative correlation (ρ=-0.22) between ADC values and Ki-67 in breast cancers (59), consistent with the findings of multiple other studies (40, 41, 43, 46, 50, 54, 55). Comparison across studies is limited, however, due to different cutoff values in the classification of high proliferation, with some using 14% and others 20%. Although statistically significant, the association is considered too weak to be clinically useful as an imaging biomarker in this context.

Histogram analysis of ADC was performed by a few groups to capture tumor heterogeneity and to determine if additional metrics were associated with prognostic factors. A study by Horvat et al. showed that the maximum ADC value based on a two-dimensional (2D) ROI on the whole tumor differentiated luminal from non-luminal cancers with an AUC of 0.685 (37). Significant overlap in ADC values between subgroups was also shown in this study, but results suggest that whole tumor segmentation may better reflect tumor heterogeneity and the different underlying architecture among molecular subtypes. Another study evaluated the added value of the entropy of ADC values, a measure of the variation in the volumetric ADC histogram and a potential surrogate for underlying microstructure heterogeneity. Results showed that the ADC entropy values differed among Luminal A, Luminal B, and triple negative phenotypes (48).

Peritumoral edema associated with breast cancer has been reported to correlate with aggressiveness and portend a poor prognosis (60–62). It has been hypothesized that neovascularity and increased vascular permeability associated with aggressive malignancies are responsible for the peritumoral edema seen on MRI (62). Therefore, evaluation of the peritumoral region may contribute additional pathophysiologic information. A study by Okuma et al. investigated whether the peritumor/tumor ADC ratio correlated with prognostic factors and indexes (49). Results showed a positive correlation between the peritumoral/tumoral ratio and size, grade, proliferation index, lymph node involvement, and lymphovascular invasion (49). While the ratio correlation of peritumor/tumor ADC with the Nottingham Prognostic Index (NPI) (0.5) and PREDICT (0.44) was stronger than that of tumoral (-0.28 and –0.25, respectively) or peritumoral (0.27 and 0.19, respectively) ADC values alone, the correlation was still considered limited to moderate. Additional studies are needed to determine if the peritumoral/tumoral ADC ratio provides any value in the prognostication of breast cancer (49).

Predicting and Monitoring Treatment Response

Neoadjuvant chemotherapy (NAC) is commonly used in the treatment of locally advanced or large breast cancer to downstage the disease and potentially allow for breast-conserving therapy (63). The ability to non-invasively evaluate treatment response not only impacts clinical management, but also confers prognostic information, with improved outcomes seen in patients with complete pathologic response. DCE-MRI is the most commonly used modality to evaluate treatment response but is limited in the ability to differentiate residual tumor from treatment related changes, including scarring, necrosis, and reactive inflammation (64). DWI offers a potential alternative or complementary technique to overcome those limitations. The cytotoxic effects of chemotherapy disrupt cell membranes and decrease tumor cellularity, which theoretically should result in increased ADC values.

Multiple meta-analyses found that DWI could detect pathologic complete response (pCR) with a pooled sensitivity and specificity of 0.8-0.89 and 0.72-0.85, respectively (65–67). The criteria used to define complete pathologic response differed among the included studies, which partially limits comparison. The DWI metrics also varied, with some studies using the change in ADC (ΔADC) with treatment, pre-treatment ADC, post-treatment ADC, or a combination of all three to determine treatment response. Chu et al. compared the different metrics and found that the pooled specificity of the ΔADC was comparable to the post-treatment ADC, but significantly higher than that for the pre-treatment ADC group (67). This finding is partially supported by the mixed results from multiple smaller studies that investigated the ability of pre-treatment ADC to predict treatment response (68–73). While this suggests that pre-treatment ADC values may not represent as reliable a predictor of pCR compared to the ΔADC and post-

treatment ADC, multi-center trials with larger population sizes and standardized acquisition protocols would be needed to make this determination and validate the use of ADC for this clinical use.

The results from the American College of Radiology Imaging Network (ACRIN) 6698 trial further demonstrate the ability of DWI to predict pathologic response (74). In this clinical trial, 272 women with breast cancer underwent DW-MRI prior to NAC, 3 weeks into treatment, 12 weeks into treatment, and after completion of chemotherapy. The percent change in tumor ADC from baseline was measured at each time point. Results showed that the ΔADC was somewhat predictive of pCR at mid-treatment (12 weeks) (AUC 0.6; 95% CI: 0.52-0.68; P= 0.017) and after treatment (AUC 0.61; 95% CI: 0.52-0.69; P = 0.013). Significantly increased treatment related ΔADC values in patients with pCR supports the findings from multiple single center studies (68, 69, 72, 75–77).

A meta-analysis by Gu et al. evaluated the role of MRI in the detection of pCR after neoadjuvant treatment in patients with breast cancer and found that DCE-MRI demonstrated superior pooled specificity in terms of identifying residual tumor (0.92 versus 0.85) while DWI maintained higher sensitivity (0.93 versus 0.64) (65). The relatively low sensitivity of DCE-MRI may be secondary to nonspecific contrast enhancement from post-treatment changes, including reactive inflammation, necrosis, and perilesional edema, or from co-existing DCIS (65). The diagnostic accuracy of DCE-MRI was greater than ultrasonography and mammography (0.96 versus 0.66 and 0.53) but not significantly different than PET/CT (0.99), which demonstrated higher sensitivity of 0.9 (65). Results suggest that DCE-MRI combined with DWI or PET/CT in these patients may improve predictive accuracy (65).

VALIDATION AND TECHNICAL CONSIDERATIONS

Technical validation is necessary prior to translation of quantitative imaging biomarkers into community practice. This process involves standardization of acquisition protocols and demonstration of acceptable repeatability and reproducibility to ensure consistent results across practice settings.

Repeatability and Reproducibility

For implementation in clinical practice, a quantitative imaging biomarker should demonstrate high accuracy and precision, reflected in repeatability and reproducibility. Repeatability represents the precision of repeated measures taken under identical conditions in a short amount of time, while reproducibility represents the precision of repeated measures wherein some aspect of the procedure is changed (e.g. different field-strength scanners) (78). Understanding the factors which affect repeatability and reproducibility, such as image acquisition parameters and data analysis, is necessary for the development of a useful imaging biomarker.

Multiple small single center studies have shown good repeatability and reproducibility of ADC measurements in normal (79–82) and malignant breast tissue (80, 81, 83). The ACRIN 6698 trial evaluated the repeatability and reproducibility of ADC measurements in a multi-institution, multi-MRI platform clinical setting (84). Results demonstrated excellent repeatability [within-subject coefficient of variation = 4.8% (95% CI 4.0-5.7%)] and reproducibility [interreader intraclass correlation coefficient (ICC) = 0.92 (95% CI 0.80-0.97) and intrareader ICC = 0.91 (95% CI 0.78-0.96)] independent of field strength when using a standardized DWI protocol and quality assurance (QA) procedures (84). This study represents an important step in the validation of ADC as a quantitative imaging biomarker by showing high precision in a multi-institution setting.

The Quantitative Imaging Biomarkers Alliance (QIBA) previously excluded breast from the QIBA Profile for DWI in 2017 due to a lack of reproducibility data in the literature. In light of the increasing evidence, the QIBA added breast to the DWI Profile in 2019, providing guidance on protocol design (**Table 1**), quality assessment, and image analysis, with additional details provided in the following sections (85).

The European Society of Breast Radiology (EUSOBI), which works closely with the QIBA, created an international breast DWI working group consisting of MRI physicists, clinical breast MRI experts, and MRI vendor representatives from 16 countries (16). The group published the first consensus and mission statement in 2020, proposing acquisition parameters for DW sequences and ROI segmentation recommendations for clinical application with the goal of improving protocol standardization across institutions and attaining standardized ADC values. The group's future efforts will focus on addressing factors that alter precision and the development of quality control, with a goal of progressing towards widespread implementation of quantitative breast DWI (16).

Acquisition Techniques

The QIBA DWI profile currently recommends utilizing a single-shot echo planar imaging (ss-EPI) acquisition sequence for diffusion weighted breast imaging (85). In ss-EPI, the imaging data from all k-space is obtained with a single radio-frequency excitation, allowing for shorter acquisition time and decreased motion artifact (6, 86). However, ss-EPI is strongly affected by susceptibility artifacts and typically has low spatial resolution. These limitations can be mitigated by adequate fat suppression, use of parallel imaging, and shimming (6, 86).

Alternative acquisition techniques have emerged to address these limitations and have demonstrated potential for improved image quality in DWI breast imaging. In general, these techniques reduce the readout duration, thus shortening the time during which the signal is affected by field inhomogeneities that cause distortion artifacts.

Readout-segmented echo planar imaging (rs-EPI) is a multi-shot technique that divides k-space into multiple segments, allowing for decreased echo spacing, reduced geometric distortion, and improved resolution (87). Multiple

TABLE 1 | Protocol guidance for diffusion weighted imaging of the breast provided by the QIBA.

Field Strength	1.5 or 3 T
Acquisition sequence	Diffusion-weighted Single-Shot Echo Planar Imaging (ss-EPI)
Receive Coil type	Ideal/Target: 5-16 channel bilateral breast coil Acceptable: 4 channel bilateral breast coil
Fat Suppression	On
Number of b-values	Ideal: ≥ 4 Target/Acceptable: 3 (including one b=0-50, one 100, and one at highest b-value Acceptable: 2 (including one b=0-50 s/mm^2 and one at highest b-value)
Minimum highest b-value strength	Target/Ideal: b=600-800 s/mm^2 Acceptable: 600 s/mm^2
Diffusion directions	Target/Ideal: 3-orthogonal, combined gradient channels Acceptable: 3-orthogonal, single gradient channels
Slice Thickness	Ideal: 4 mm Acceptable: 5 mm
Gap thickness	Ideal: 0 mm Acceptable:1 mm
Field-of-view	Ideal/Target/Acceptable: 260-360 mm (complete bilateral coverage)
Acquisition matrix	Target/Ideal (128-192) x (128-192), or 2.8- 1.8 mm in-plane Acceptable: 128 x 128, or 2.8 mm in-plane resolution
Plane orientation	Transversal-axial
Half-scan factor	Acceptable/Target: >0.65
Phase-encode/frequency-encode direction	Anterior-Posterior/Right-Left or Right-Left/Anterior-Posterior
Number of averages	Ideal/Target: 3-5 Acceptable:2
Parallel imaging factor	Ideal: ≥ 2 Target/Acceptable: 2-3/2
TR	Ideal/Target/Acceptable ≥ 4000 ms
TE	Ideal/Target: minimum TE (50-100ms) Acceptable: < 114 ms
Receiver Bandwidth	Ideal/Target: maximum possible in frequency encoding direction (minimum echo spacing) Acceptable: > 1000 Hz/voxel

Definitions provided by the QIBA:
ACCEPTABLE: Actors that shall meet this specification to conform to this profile.
TARGET: Meeting this specification is achievable with reasonable effort and adequate equipment and is expected to provide better results than meeting the ACCEPTABLE specification.
IDEAL: Meeting this specification may require extra effort or non-standard hardware or software, but is expected to provide better results than meeting the TARGET.

studies have demonstrated superior breast lesion conspicuity and image quality with rs-EPI compared to ss-EPI (88–91). Inter-reader agreement of known mass and non-mass lesions was evaluated in two studies: DCE-MRI and rs-EPI collected with b-values of 0 and 850 s/mm^2 resulted in comparable morphologic lesion assessment and diagnostic performance (21, 92). These findings suggest rs-EPI as a potential alternative to DCE-MRI. However, improved image quality with rs-EPI is often at the expense of increased acquisition times, and lesion conspicuity remains inferior to DCE-MRI

Simultaneous multi-slice (SMS) rs-EPI was introduced to address the increased acquisition times required with rs-EPI. In SMS imaging, multiple slices are acquired simultaneously so that the number of excitations required for the same slice coverage is reduced (93). The spatial sensitivity of multichannel array coils is subsequently used to separate the slices acquired in parallel (93). Filli et al. first demonstrated the feasibility of SMS rs-EPI in 8 healthy volunteers, comparing conventional rs-EPI to two-fold and three-fold slice-accelerated rs-EPI (**Figure 3**) (94). They found that while scan time was significantly reduced and SNR was improved with additional acceleration, ghosting artifacts and shading in the prepectoral region were more distinct (94). A more recent study by Song et al. compared image quality, lesion conspicuity, and scan time between rs-EPI and SMS rs-EPI

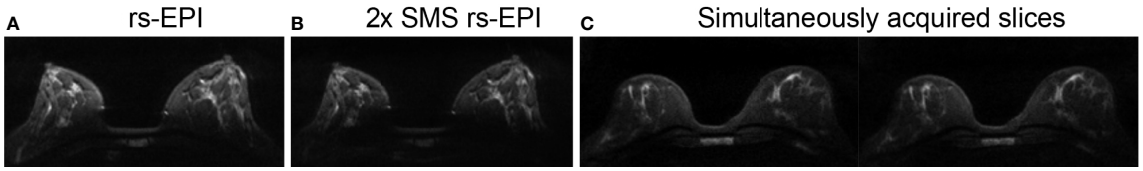

FIGURE 3 | Example of SMS rs-EPI acquisition at b=800 s/mm^2 in a 35-year-old healthy volunteer, wherein **(B)** two-fold (2×) SMS rs-EPI maintains comparable image quality as **(A)** conventional rs-EPI while reducing scan time in a 3T scanner. Panel **(C)** shows two simultaneously acquired slices used to generate a single-band equivalent image for the same patient at a different slice location (94). (Courtesy of Lukas Filli, MD, Zurich, Switzerland).

sequences in 134 women with invasive breast cancer (95). The study found a 44% reduction in scan times, improved image quality, and enhanced lesion conspicuity with SMS rs-EPI, similar to the results of a study by McKay et al. (95, 96). Compared to conventional rs-EPI, SMS rs-EPI produced comparable AUC and ADC values in multiple studies, suggestive a potential method of reducing scan time while preserving diagnostic accuracy (94, 95, 97, 98).

Reduced field of view (rFOV) improves spatial resolution and decreases artifacts by limiting the field of view and number of k-space lines in the phase-encoding direction (99, 100). Improved image quality with rFOV compared to standard DWI techniques has been shown to enhance lesion conspicuity and morphologic assessment in the breast (101–104). Significant differences in ADC values with rFOV compared to full FOV DWI, however, may limit the utility of proposed ADC cutoff values when employing rFOV techniques (**Figure 4**) (101, 102, 104, 105).

rFOV has been used in conjunction with other acquisition strategies to further improve image quality and reduce scan time. For instance, Taviani et al. developed a single-shot image-segmented technique that combines rFOV, 2D in-plane multiband radiofrequency pulses, and a generalized parallel imaging reconstruction method to generate images with high resolution and anatomical fidelity (106).

Diffusion weighted double-echo steady state (DW-DESS) imaging is an emerging technique that allows for rapid acquisition of high-resolution images by utilizing a short repetition time (TR) (107–110). The diffusion weighted DESS sequence acquires two echoes per radiofrequency pulse, during which a steady state of longitudinal and transverse magnetization is achieved. Multiple parameters affect the diffusion weighting in DW-DESS, such as the TE, TR, flip angle, spoiler gradient duration, and tissue relaxation and diffusion properties (107, 108, 110). A few studies have evaluated the use of DW-DESS imaging in the breast and found superior image quality and improved morphologic assessment when compared to conventional EPI DWI (108, 111). Benefits of this technique include rapid acquisition times and avoidance of EPI-associated distortions and blurring (107, 108). The DW-DESS sequence, however, is susceptible to motion artifacts, particularly with increased diffusion weighting (109). Moran et al. developed a DW-DESS-Cones method using a three-dimensional cones (non-cartesian) trajectory to address this limitation, and demonstrated significantly reduced motion artifacts (**Figure 5**) (109). At present, DW-DESS techniques do not provide a reliable quantitative measure of diffusion equivalent to ADC values, and will likely be the focus of future investigations (108, 109).

b-Value Selection

ADC values are typically displayed as a parametric ADC map. Regions of high cell density and hence highly hindered and restricted (including partially restricted) diffusion appear hypointense on the ADC map and hyperintense on high b-value diffusion weighted images.

According to the monoexponential mathematical model (Eqn. 1), b-value selection directly affects the ADC value, signal-to-noise ratio (SNR), and contrast-to-noise ratio (CNR). With increasing b-value, ADC values theoretically decrease due to the predominance of non-Gaussian diffusion. Additionally, increased CNR with increasing b-values may improve lesion detection at the expense of decreased SNR (10). Studies aiming to identify optimal b-value selection in DWI of breast demonstrate varied results (112–115). The QIBA requires a minimum of two b-values, b=0-50 s/mm^2 and b≥ 600 s/mm^2, but recommends ideally acquiring 4 or more b-values, including b=0-50 s/mm^2 (78). As more evidence emerges, particularly with advanced modeling techniques requiring multiple b-values, recommendations may become increasingly specific.

ROI Delineation

Typically, ADC values are extracted by placing a region of interest (ROI) on the restricting lesion. The most commonly employed methods of ROI placement are whole lesion

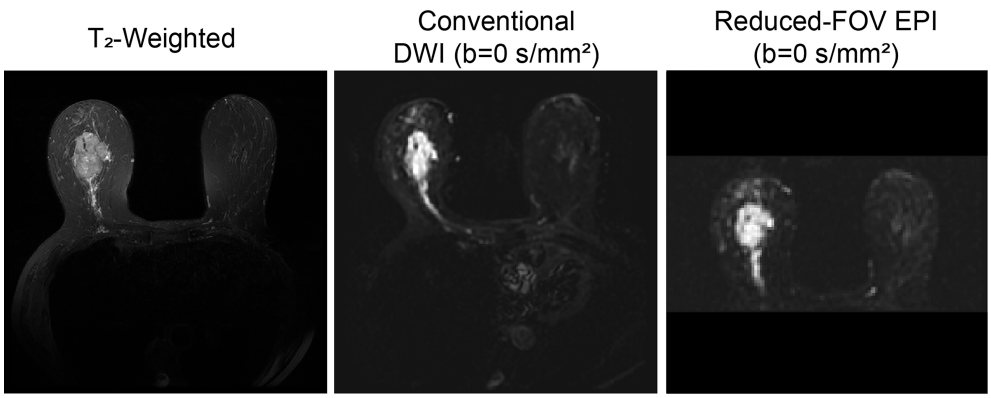

FIGURE 4 | Reduced FOV EPI in a 63-year-old patient with invasive ductal carcinoma. T_2-weighted, conventional DWI (b=0 s/mm^2), full FOV EPI (b=0 s/mm^2), and reduced FOV EPI (50% phase field of view) (b=0 s/mm^2 acquired at 3T) images are shown. Reduction of percent phase encoding direction to 50% reduces geometric distortions caused by B_0-inhomogeneity, especially in the nipple region (100).

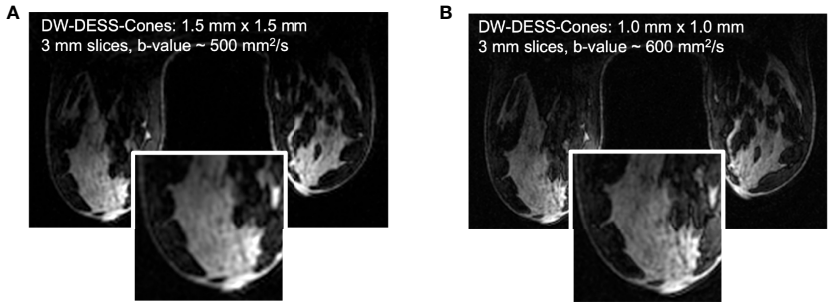

FIGURE 5 | Based on the results of the initial DW-DESS-Cones investigation in the breast at 3T **(A)**, the diffusion-weighting and resolution of the method can be further increased **(B)** to better match contrast and resolution expectations for breast MRI (109). (Courtesy of Catherine Moran, PhD, Department of Radiology, Stanford University, Stanford, California, USA).

segmentation and focused segmentation, where the ROI is applied to the most restricting portion of the lesion (highest signal on DWI corresponding to lowest ADC value on ADC maps) (116–119). ROI placement has been shown to significantly affect ADC measurements, limiting the use of proposed ADC cutoff values (116–119). Compared to whole lesion segmentation, focused ROI placement demonstrates superior diagnostic accuracy in the evaluation of breast lesions in a few studies, likely on the basis of emphasizing the most restricting and thereby most suspicious portion of the tumor (117, 119). Focused segmentation allows the exclusion of region of necrosis, non-enhancement, and artifacts, resulting in an ADC value that may better represent the underlying microstructure (16, 118). Additionally, semiautomated ROI delineation algorithms, such as that developed by Rahbar et al., can improve inter-reader reproducibility of ADC measures (120). While the QIBA has not provided ROI placement standards, the EUSOBI presently recommends using a focused segmentation method—while taking care to avoid regions of necrosis, non-enhancement, and artifacts—with the goal of improving consistency of DWI across institutions (16).

ADVANCED AND EMERGING TECHNIQUES

To address the shortcomings of the monoexponential ADC model in capturing the complex tissue micro-structure in the breast, several advanced diffusion models have been developed and will be explored in this section.

Diffusion Tensor Imaging

Diffusion tensor imaging (DTI) is a quantitative technique within DWI that measures the diffusion directionality (anisotropy) of water molecules by applying at least 6 directional diffusion gradients, providing a three-dimensional representation of diffusion (121–125). The diffusion tensor model is mathematically represented by a symmetric matrix of six parameters: three orthogonal eigenvectors (v_1, v_2, v_3), reflecting the direction of diffusion, and three corresponding eigenvalues (λ_1, λ_2, λ_3), reflecting the degree of diffusion in each orthogonal direction (121–125). From the eigenvalues, DTI metrics are derived (121, 125). The most common DTI metrics studied are fractional anisotropy (FA), or the fraction of diffusion that is anisotropic on a scale from 0 to 1, and mean diffusivity (MD), or the average of tensor's eigenvalues, also represented as the ADC (121, 125). Additional DTI parameters include maximal anisotropy (MA), relative anisotropy (RA), volume ratio, geodesic anisotropy, and radial diffusion. Maximal anisotropy represents the difference between the highest and lowest value of anisotropic water movement (λ_1 - λ_3) (126). Relative anisotropy is the ratio of the standard deviation to the mean of the three eigenvalues, ranging from 0 to $\sqrt{2}$, with 0 representing isotropic diffusion and the $\sqrt{2}$ representing diffusion in a single direction (126). The volume ratio is the ratio of the ellipsoid to spherical, ranging from 0 to 1, with 1 reflecting isotropic diffusion (127). Radial diffusivity is the average of the two smaller eigenvalues (λ_2 and λ_3) (128)

Normal breast architecture is comprised of multiple lobules with a complex ductal network with surrounding fibrous stroma and intervening fatty tissue. Within small ducts, it has been suggested that the diffusion of water molecules is anisotropic and DTI values may provide information regarding pathophysiologic changes in tissue microstructure (123, 129). A few studies have evaluated DTI parameters in women with normal breasts and found significant regional differences, with increased FA within the periphery and posterior aspects of the breast compared to the central breast, which is postulated to reflect anisotropic diffusion within smaller, collapsed ducts peripherally and posteriorly (123, 129, 130). A study by Plaza et al. showed no association between DTI parameters and fibroglandular tissue composition, but found a significantly lower λ_1 in normal breasts with moderate/marked background parenchymal enhancement (BPE) compared to those with minimal/mild BPE (131). Other studies have observed that DTI parameters are resistant to physiologic differences in breast tissue composition due to their unique ability to track underlying ductal microstructure (123, 132, 133). In comparison to DCE, certain DTI parameters have also shown superior tumor conspicuity in lactating patients with pregnancy-associated breast cancer (134). Background parenchymal enhancement is a challenge among this patient population. In a study by Nissan et al., CNR for lactating

patients with pronounced BPE were higher on λ_1, λ_2, λ_3, and MD (1.81 ± 0.67, 1.95 ± 0.87, 1.79 ± 0.83, respectively) maps as compared with those of DCE images (0.82 ± 0.49) ($p < 0.005$, for all) (134). These correspond to an increase in CNR of up to 138% by DTI-derived parameters, compared to DCE. DTI parameters, much like ADC (132, 135–137) have been shown to be resistant to changes in the breast parenchyma (131, 132, 134), unlike DCE (138, 139), which further demonstrates the utility of diffusion MRI as an effective adjunct to DCE.

Disruption of the breast architecture has been suggested to alter anisotropic indices, and which may therefore serve as potential imaging biomarkers of malignancy. A comprehensive meta-analysis by Wang et al. evaluated the diagnostic performance of DTI metrics in discriminating benign versus malignant breast lesions (140). This analysis included 16 studies with a total of 1636 patients and found significantly higher FA (0.15-0.55 versus 0.02-0.13), and lower MD (0.71-1.62 versus 1.08-1.91), λ_1 (0.97-1.62 versus 1.19-2.15), λ_2 (0.95-1.29 versus 1.50-1.68), and λ_3 (0.78-1.12 versus 1.20-1.56) in malignant lesions compared to benign lesions (140). Decreased diffusion coefficients may be in part secondary to increased cellularity within the malignancy, as well as ductal involvement of neoplastic cells (140). Pooled FA was increased in malignant lesions, but individual studies showed conflicting results (140). For example, Furman-Haran et al. found no difference in FA between malignant lesions and contralateral breast parenchyma, but did find that the absolute maximal anisotropy index (λ_1-λ_3) differentiated the tissues (lesion: 0.51 x 10−3, mm2/sec, versus normal: 0.84 x 10^{-3} mm^2/s, $p<0.001$) (126). Increased FA values in malignancy are postulated to reflect disorganized architecture with regional necrosis or hemorrhage, that results in increased diffusion along certain directions but hindered diffusion in others (126, 140). If regions of necrosis or hemorrhage are large enough, however, diffusion of water molecules may be uninhibited and result in reduced anisotropy, which may explain why some of the included studies concluded that FA could not distinguish malignant from benign lesions (140). Furthermore, normalized anisotropic indices such as FA are subject to the inherent mean diffusivity of the underlying tissue, which may differ by lesion subtype (126, 140). Subgroup analysis revealed a significantly lower MD value among invasive breast cancer lesions compared to DCIS (140). Overall, λ_1 demonstrated the highest diagnostic accuracy, with a pooled sensitivity of 93%, specificity of 92% and AUC of 97%. These findings suggest MD and λ_1 may be clinically useful markers of malignancy (123, 128, 140, 141).

An additional meta-analysis performed by Baxter et al. compared the diagnostic performance of DWI, DTI, and intravoxel incoherent motion (IVIM) in the characterization of breast lesions (29). In this analysis, λ_1 also demonstrated the highest diagnostic accuracy among DTI metrics, with a pooled sensitivity of 93%, specificity of 90% and AUC of 94% (29, 123, 128, 141). Overall, the diagnostic performance of DWI, DTI and IVIM was comparable but the conclusions were limited by the low number of included studies and thereby low statistical power (29).

The association of DTI parameters with prognostic factors has been investigated by a few studies with promising results (128, 142–144). Significantly low MD and FA values were found to correlate with larger tumor size (>2 cm), high histologic grade, and axillary nodal metastases/lymphovascular invasion (142–144). Other DTI parameters were also found to be significantly associated with ER, PR, CERB-B2, Ki-67 and intrinsic subtypes (128, 143).

A retrospective study by Furman-Haran et al. included 20 women undergoing NAC and compared DTI parameters with DCE-MRI in the ability to monitor treatment response (145). Results showed that the post NAC change in multiple DTI parameters, including MD, λ_1, λ_2, and maximal anisotropy (λ_1-λ_3) differentiated responders from non-responders after NAC, with the highest AUC seen with MD, λ_1 and λ_2 (145). The change in FA was not statistically significant (145). Pre-NAC DTI parameters however showed low diagnostic performance in the ability to predict NAC response (145). Tumor size changes following NAC measured by DTI were of comparable accuracy to that of DCE and found to also be a significant discriminator between responders and non-responders (145). Residual tumor diameter correlated well with the postoperative pathological tumor diameter (145).

At present, no standard DTI protocol exists, with varied selection of b-values and numbers of diffusion gradients seen across studies, which may affect the resultant DTI metrics. It has also been demonstrated that DTI is prone to artifacts at high b-values and high resolution, common to other EPI-based sequences, which affect interpretation of the DTI parameters (146). A study by Yamaguchi et al. found superior diagnostic performance of DTI based on rs-EPI compared to DWI based on ss-EPI, which was attributed to improved lesion conspicuity and diminished blurring artifact (144). Further studies are needed to establish a standardized protocol and threshold values for practical clinical use.

Intravoxel Incoherent Motion (IVIM)

Diffusion-weighted imaging and subsequent ADC measurement are influenced by both Gaussian and non-Gaussian diffusivity, which includes microcapillary perfusion. The intravoxel incoherent motion (IVIM) model, first introduced in 1986 by Le Bihan et al., provides a method to separate the contribution of micro-perfusion from tissue diffusivity to the diffusion-weighted signal (147). Using the following biexponential decay model,

$$S/S_0 = fe^{-b(D+D*)} + (1-f)e^{-bD} \quad [2]$$

and multiple b-values, the following parameters can be attained: water diffusion through tissue (D or D_t), pseudo-diffusion from perfusion (D^*, D_p or D_f) and the perfusion fraction (f, f_p, or f_{IVIM}). First applied to the breast in 2011 by Sigmund et al., the IVIM model has been increasingly studied and shown promise in the evaluation of breast lesions (148).

The IVIM parameters have been shown to aid in the discrimination of malignant from benign breast lesions. In multiple studies, malignant lesions showed significantly decreased tissue diffusivity (D_t) values and increased perfusion fraction (f_p) values compared to benign lesions and normal

breast parenchyma (36, 149–162). A recently published review of fifteen studies yielded sensitivity of 87 ± 10% and specificity of 79 ± 17% for D_t in malignant lesions, and a sensitivity of 81 ± 7% and specificity of 75 ± 3% for f_p (163). In terms of diagnostic performance, multiple studies found that at least one IVIM metric, most consistently D_t, outperforms ADC, with one study finding an increased AUC when D_t and f_p are combined (0.84 vs 0.75 for D_t alone, and 0.79 for f_p alone) (**Figure 6**) (36, 152–155, 157–159).

Direct comparison and correlation of IVIM parameters with standard DCE-MRI has been performed (155, 157, 165). In a few studies, D_t outperformed DCE-MRI derived parameters with an overall increased AUC when IVIM and DCE-MRI parameters were combined (AUC 0.99 with combination of D_t and time-signal intensity curve (157); AUC 0.93 with multivariate combination of IVIM and DCE parameters (155, 157, 165). Multiparametric approaches combining IVIM and other non-Gaussian DWI parameters also have shown increased diagnostic accuracy, with one study by Lima et al. demonstrating BI-RADS equivalent scores (150). These findings suggest that the addition of IVIM metrics to standard DCE-MRI may improve diagnostic accuracy, and that IVIM may represent a non-invasive alternative to DCE-MRI.

The role of IVIM in the non-invasive identification of prognostic factors in breast cancer has also been investigated. Multiple studies found a correlation between D_t and ER expression (36, 56, 161, 166). Zhao et al. also found that the D* and D_t significantly correlated with ER and PR expression and Luminal A subtypes (161). Luminal B subtypes in this study showed significantly decreased f_p, with significantly diminished peritumoral f_p values among HER2 positive lesions compared to HER2 negative lesions, a finding which may reflect diminished central perfusion secondary to intratumoral necrosis (161). The IVIM parameters D*, f_p and D_t correlated with TNBC status, with increased f_p values along the tumor edge compared to other subtypes and increased peritumoral D* values, which may suggest a high degree of invasiveness (161). The work by Zhao et al. showed that applying IVIM metrics to the peritumoral and tumor edge may shed light on the underlying pathophysiology.

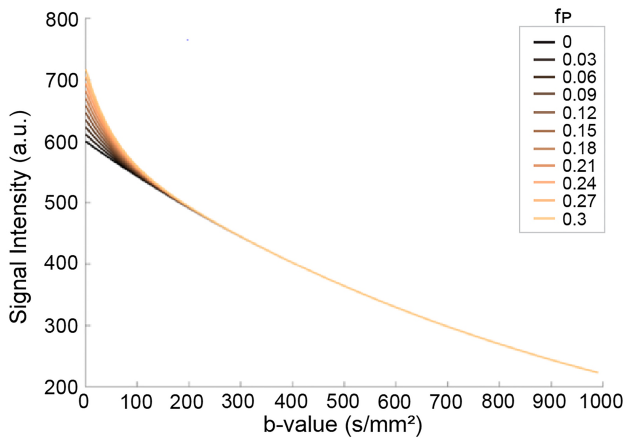

FIGURE 6 | Effects of pseudo-diffusion on DWI signal. Signal curves in the presence of increasing IVIM effects deviate from the simple mono-exponential curve (f_p=0, black line). The components have unique coefficients D_t = 0.001 s/mm^2 and D* = 0.02 s/mm^2 with relative proportions given by the pseudo-diffusion fraction f_p (164). (Courtesy of Igor Vidić, PhD, previously at the Department of Physics, Norwegian University of Science and Technology, Trondheim, Norway).

Multiple studies found a correlation between D_t values and Ki-67 expression (149, 161, 162, 167, 168), with two of these studies demonstrating a correlation with f_p values (161, 168). Evaluation of the association of IVIM metrics with lymph node metastases and histologic grade, however, have yielded conflicting results (56, 159, 161, 166, 168).

A study by Lee et al. investigated the association of IVIM parameters with two markers of tumor angiogenesis, microvascular density (MVD) and vascular endothelial growth factor (VEGF), in patients with breast cancer using 4 different curve fitting algorithms (169). The authors found significant associations between multiple perfusion related parameters and VEGF using a linear regression model to determine D_t and f_p at high b values, and linear regression to determine D* at low b values (≤50 s/mm^2) (169). However, no association was found between MVD and IVIM parameters obtained by the 4 different curve fitting algorithms, and additional studies are needed to determine if there is a correlation (169).

Histogram analysis of IVIM parameters performed by a few groups demonstrated the potential to distinguish breast cancer subtypes and additional prognostic factors (36, 166, 170). As opposed to the majority of studies where the average values for IVIM metrics are obtained, histogram analysis appears to provide additional information of the distribution of the metrics, including skewness and kurtosis, which better reflect tumor heterogeneity.

A few studies evaluating the ability of IVIM parameters to predict treatment response have shown conflicting results. Two studies reported increased D_t values following NAC in the responder (or pCR) group (171, 172), whereas two other studies did not find significant differences between groups (70, 173). The small sample sizes in these studies may account for the observed differences, warranting further investigation with larger cohorts.

Direct comparison across studies is limited due to the variability in the methods of image acquisition and data analysis, as the choice of curve fitting methods and b-values have been shown to affect IVIM metrics (174, 175).

The b-value selection significantly affects IVIM metrics. A threshold value of 200 s/mm^2 has been used, with perfusion effects predominating below 200 s/mm^2 and diffusion effects predominating above 200 s/mm^2 (150, 151, 153, 174). However, a variety of threshold b-values have been used in breast studies and there is currently no consensus on the optimal threshold or b-values choice. A study by Chen et al. aimed to determine the optimal threshold b-value and found an optimal cutoff value of 300 s/mm^2 discriminated diffusion from perfusion effects (176). Ongoing research efforts aim to determine the optimal b-values. For example, Cho et al. compared a free (conventional constrained least squares fit) versus a segmented (two step

constrained analysis) fitting method for both conventional or optimized b-values (174). This group found that the IVIM values differed significantly according to the sampling method, with a segmented method for optimized b-values showing the highest accuracy and precision (174).

Several studies have investigated different fitting and analysis methods for IVIM in order to increase accuracy and differentiation between lesion type. Suo et al. compared three frequently used calculation methods in women with biopsy proven IDC and found significantly higher precision when using either of the applied two step calculation methods compared to the conventional free fitting model (175). Most IVIM metrics differed significantly according to the calculation method, with a significantly larger f_p value with the free fitting model (175).

Bayesian fitting approaches have been investigated as an alternative to nonlinear least squares fitting (177, 178). The Bayesian model uses prior knowledge or assumptions of the system to provide estimates of IVIM parameters for pixels with a high degree of data fitting uncertainty, decreasing heterogeneity in the parameter maps (177). A study by While et al. compared the performance of multiple Bayesian modeling approaches with least squares-based approaches on simulated breast and liver tissue (177). In terms of relative error and estimator deviation, Bayesian approaches outperformed both full and segmented least squares-based methods (177). However, in areas of high parameter uncertainty, certain features disappeared, potentially masking important tissue characteristics and limiting interpretation (177). This study also showed that segmented least squares approach was superior to the full nonlinear approach in the breast (177).

Alternative methods of data analysis have been proposed. In one such method called the exhaustive approach, the parameters are derived from comparing the raw signal to an exhaustive database of simulated signals, comprised of a large set of parameter combinations (153). This method may provide a better estimation of IVIM metrics by eliminating the local minima issue seen in fitting models, but it requires high processing power (153). An additional method, termed the simplified approach, uses only three b-values to calculate the relative enhanced diffusivity (RED), a metric that pools the effects of ADC mapping and IVIM modeling (179, 180). A study by Teruel et al. found that the RED differentiated malignant from benign breast lesions with an overall accuracy of 90% using b-values of 0, 200 and 700 s/mm^2 (180).

Diffusion Kurtosis Imaging (DKI)

Diffusion kurtosis imaging (DKI) is an extension of DWI in which both Gaussian and non-Gaussian diffusion distributions are quantified, providing added insight into the tissue microstructure (181). DKI yields the parameters mean diffusivity (D), representing Gaussian diffusion, and mean kurtosis (MK, K), a unitless metric representing the degree of non-Gaussian diffusion. The DKI model is the following:

$$\ln \frac{S(b)}{S(0)} \approx -bD + \frac{1}{6} b^2 D^2 K \quad [3]$$

where S(b) is the DW signal with non-zero diffusion weighting, S (0) the signal without diffusion weighting, and b the diffusion weighting factor (181). As malignant lesions proliferate, increased cellularity results in decreased extracellular space and increased microstructural complexity (i.e. cell membranes and organelles), impairing Gaussian diffusion (182). The degree of deviation from Gaussian diffusion can be quantified by K, with increasing K value reflecting increasing deviation (**Figure 7**) (181).

The potential of DKI parameters in the characterization of breast lesions has been investigated. Multiple studies have found that malignant lesions demonstrate a significantly higher K (0.61-1.13) and lower D (1.01-1.52 × 10^{-3} mm^2/s) values compared to benign lesions (K of 0.37-0.69; D of 1.52-2.17 × 10^{-3} mm^2/s) (56, 150, 153, 182–188). Further, DKI studies have also shown promise in the K value for differentiating breast lesion types, as K was significantly higher in invasive cancers (0.93-0.94) compared to DCIS (0.78-0.81) (56, 188). Nogueira et al. found that K could differentiate a fibroadenoma from fibrocystic change (0.48 vs 0.25) (184).

Histogram analysis has been applied to the kurtosis model in two studies, in which it was found that histogram metrics within each individual group outperformed the mean values, which are typically used in standard diffusion kurtosis imaging (185, 189). Visualization of tumor heterogeneity *via* histogram analysis may result in identification of the most aggressive portions of the lesions and therefore increase diagnostic accuracy in the discrimination of benign and malignant lesions.

In terms of diagnostic performance, few reporting studies demonstrated a high AUC for both D and K in discriminating benign from malignant lesions (153, 182–184). Compared to ADC, kurtosis metrics in some studies demonstrate increased superior diagnostic performance (190), while in others, there was no significant difference (56, 187, 191).

The association of prognostic factors with kurtosis metrics has also been investigated, with studies yielding conflicting results. A few studies found a positive correlation between K and high histologic grade (186, 187, 190), while others showed no association (56, 191). Others also showed significantly increased K value with elevated Ki-67 expression (168, 186, 187, 190), while one found no significant association (108). Studies evaluating the correlation between kurtosis metrics and hormone receptor expression, HER2 status, and lymph node involvement also show varying results (56, 168, 186, 190).

The ability of DKI metrics to predict recurrence risk of breast cancer was evaluated by Wu et. al, and a significant difference was found among multiple histogram kurtosis metrics (D_{mean}, $D_{50\%}$, K_{mean}, $K_{30\%}$, $K_{50\%}$, $K_{70\%}$) and the low, intermediate and high RS groups (192). Specifically, the $K_{50\%}$ demonstrated the strongest correlation with risk scores and showed potential as a biomarker for the prediction of breast cancer recurrence.

Overall, the mixed performance of DKI in discriminating lesion malignancy and subtypes warrants critical evaluation into the sources of discrepancies prior to translation into clinical practice. For instance, Mlynarska-Bujny et al. found that residual fat signal from incompletely fat-suppressed DWI images significantly reduced the diagnostic performance of DKI measures

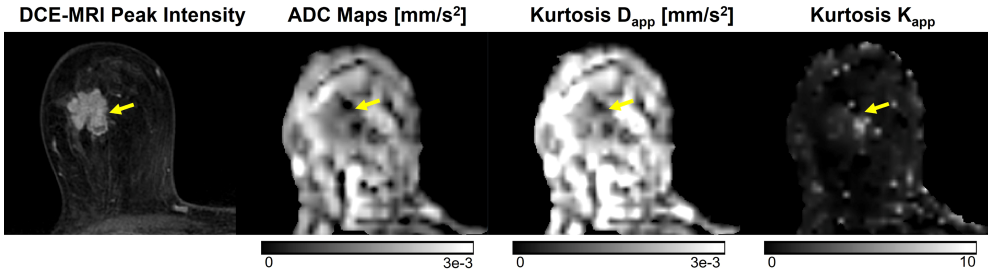

FIGURE 7 | Example of DKI analysis using b-values of 0, 500, 1000, and 2000 s/mm^2, compared to conventional ADC images using b-values of 0 and 1000 s/mm^2 and DCE-MRI peak intensity subtraction (1 min 30 s post-contrast). Invasive ductal carcinoma in a 67-year-old patient is indicated by the yellow arrow. The lesion displays higher mean kurtosis (K_{app}) than surrounding healthy tissue. Images were acquired using a wide-bore 3T scanner, and mean kurtosis and diffusivity (D_{app}) were calculated as previously demonstrated (181).

and proposed an additional fat correction term to account for fat-related signal contamination (193). Differences in experimental technique (e.g., diffusion time interval), analysis method, ROI selection, and subject variability seem to considerably influence DKI measures. Low SNR from high b-values and long scan times from an increased number of b-values needed for kurtosis modeling have also contributed to fewer clinical studies evaluating DKI (194). Future studies should aim to characterize the variation in DKI across acquisition parameters and provide recommendations for a standardized protocol.

Synthetic ADC (sADC)

There are several techniques where collecting multiple b-values is desired, however this process consumes scan time. Synthetic or shifted ADC (sADC), potentially addresses the issue of increased scan time by calculating the sADC at two shifted b-values, typically 200 s/mm^2 and 1500 s/mm^2, with the aim of capturing both Gaussian and non-Gaussian diffusion (150). A reader study conducted by Iima et al. compared sADC (using b-values=200 and 1500 s/mm^2) to two integrated diagnostic approaches (combined thresholds approach using IVIM and kurtosis parameters and a Bayesian approach) in the characterization of breast lesions (150). The "combined thresholds" approach calculated the K and ADC at b=0 s/mm^2 using the kurtosis model and combined them with f_{IVIM} to create a single metric comparable to the BI-RADS score. The Bayesian approach used the f_{IVIM}, ADC_0 and K within each individual lesion to create a probability for BI-RADS categories. The three approaches had high positive predictive value (for radiologists A and B, respectively: combined thresholds, 92.3% and 90.1%; Bayesian approach, 94.6% and 89.7%; and sADC approach, 92.3% and 93.2%), comparable with BI-RADS (93.8%) (150). Furthermore, sADC values differed significantly according to histologic subtypes (P = 0.006). While sADC did not demonstrate higher overall diagnostic performance compared to BI-RADS, the results of the study indicate the parameter's potential as a non-contrast diagnostic tool. Another study by Choi et al. compared synthetic DWI at b-values of 1000 and 1500 s/mm^2 with conventional DWI at b-values of 800 and 1500 s/mm^2 in a group of 50 individuals with breast cancer (195). $sDWI_{1500}$ showed increased lesion conspicuity compared to conventional DWI_{1500}, similar to the results of a study by Bickel et al. (196). Although $sDWI_{1500}$ demonstrated decreased overall image quality compared to conventional DWI_{1500}, the difference in cancer detection rate was not statistically significant (195). While sADC may demonstrate potential as a rapid alternative to DCE-MRI or conventional DWI, larger studies are needed to better evaluate its diagnostic performance in the breast. The limitation of the synthetic higher b-value is that although it may improve tumor conspicuity, it does not reflect true physiologic assessment associated with real higher b-value data.

Stretched Exponential Model

The stretched exponential model is another emerging non-Gaussian diffusion technique that provides added information about diffusion heterogeneity. Parameters include the distributed diffusion coefficient (DDC), which represents the mean intravoxel diffusion rate, and alpha (α), a value between 0 and 1 which quantifies the degree of deviation from monoexponential behavior. An alpha value of 1 represents pure Gaussian diffusion whereas lower values represent diffusion heterogeneity and represent a potential surrogate for tissue complexity (56). Significantly lower DDC and alpha values have been demonstrated in malignant lesions (DDC: 0.72-1.00 $\times$ 10^{-3} mm^2/s, α: 0.62-0.78) compared to benign lesions (DDC: 1.22-1.84 $\times$ 10^{-3} mm^2/s, α: 0.67-0.90) and normal breast tissue (DDC: 1.38-1.83 $\times$ 10^{-3} mm^2/s, α: 0.74-0.86) (**Figure 8**) (56, 197–200). A few studies have also demonstrated that DDC can discriminate invasive breast cancer from DCIS (56, 199) (56).

A study by Suo et al. compared the diagnostic utility of the monoexponential, biexponential, stretched exponential, and kurtosis models in the evaluation of breast lesions (56). The group found a negative correlation between alpha level and tumor size and Ki-67 expression, which is consistent with the hypotheses that larger tumors and those with higher Ki-67 expression (a marker of cellularity) demonstrate increased microperfusion and microstructural heterogeneity. The study also found significantly lower DDC values for ER positive tumors compared to ER negative tumors (0.68 versus 0.77) (56).

Regarding goodness-of-fit assessment, the kurtosis model best characterized benign voxels, while the stretched exponential model best characterized malignant voxels. Though multiple non-monoexponential parameters correlated significantly with malignancy, the diagnostic accuracy was not superior to conventional ADC, suggesting that these metrics may provide additional information for tissue characterization but that ADC may remain the standard for breast cancer diagnosis (56).

Signature Index

Another diffusion weighted technique which may mitigate the issue of complex post-processing and long acquisition times is the Signature index (s-index) proposed by Goto et al., which requires acquisitions at only 3 b-values (201). The S-index is a model free parameter derived from the difference in signal between the tissue in question and a library of reference DW signals for both malignant and benign lesions at two key b-values (201). Using this method, the authors reported comparable diagnostic performance of the S-index and sADC in the discrimination of malignant and benign breast lesions (201). The combination of the S-index with BI-RADS showed the highest diagnostic accuracy. The S-index was also found to correlate with HER2 status and PR expression. One potential drawback is that some of the specificity afforded by individual parameter values that reflect either microvascular or structural changes is lost with the S-index (201).

Restriction Spectrum Imaging (RSI)

Restriction spectrum imaging (RSI) is an emerging advanced DWI technique that aims to characterize tumor microenvironment based on the behavior of water molecules in different tissue-specific water pools (202–204). The RSI model requires multiple b-values (including b-values up to 4000 s/mm^2) and diffusion directions at a fixed diffusion time in order to produce maps that differentiate: [1] isotropic restricted (intracellular), [2] anisotropic hindered (extracellular), and [3] free water diffusion compartments (5). This distinction allows for the isolation of diffusion related changes secondary to peritumoral edema or necrosis, which often confounds standard ADC measurements, particularly in the evaluation of aggressive malignancies. In a small group of patients with high grade brain tumors, RSI improved lesion conspicuity and delineation compared to standard DWI (5). Additionally, in the evaluation of tumor response to antiangiogenic treatment in a group of patients with recurrent gliomas, RSI was less affected by medication-induced alterations in edema when compared to ADC, potentially addressing the issue of pseudoresponse and providing a method to identify true tumor response (5).

While initial oncologic applications were in the brain and prostate, the potential role of RSI in breast cancer is actively being explored. Rodríguez-Soto et al. found that a three-component (tri-exponential) RSI model better discriminates malignant lesions from healthy fibroglandular tissue compared to a bi-exponential model and conventional ADC, with similar tumor conspicuity as DCE-MRI (205). In the tri-exponential RSI breast-specific model, the main outputs are signal contribution maps of each compartment C_1, C_2 and C_3. The signal contributions from slow diffusion compartments (C_1 and C_2) were larger in malignant lesions than they were in healthy tissue (**Figure 9**) (205). In another study, Andreassen et al. utilized the three-component RSI model to characterize breast lesions in a group of 106 women with pathology-proven breast cancer (206). In this study, the RSI derived parameter C_1C_2, representing the product of the signal contributions of the slowest components C_1 and C_2, demonstrated comparable diagnostic accuracy to DCE-MRI, with an AUC of 0.984 (206). The false positive rate, given a sensitivity of 80% ($FPR_{80\%}$), of the C_1C_2 parameter (0.016) was significantly lower than that of conventional ADC (0.731) and K (0.684) (206). It is hypothesized that the higher discriminatory performance of C_1C_2 could be attributed to the ability of this parameter to suppress signal from both fibroglandular and fatty

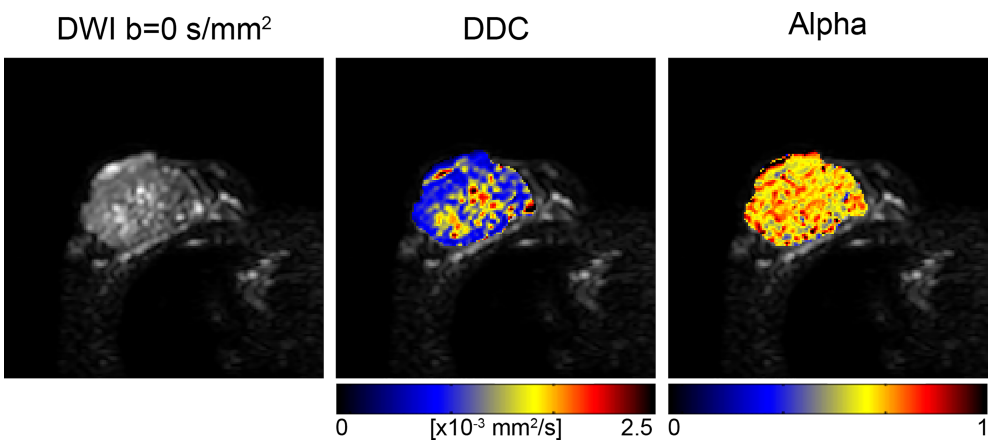

FIGURE 8 | Stretched exponential modeling with b-values of 0, 500, 1000, 1500 and 2000 s/mm^2 in a 73-year-old patient with invasive ductal carcinoma. Distributed diffusion coefficient (DDC) and alpha maps are overlaid on DWI b=0 s/mm^2 images, acquired at 3T (56). (Courtesy of Shiteng Suo, PhD, and Jia Hua, MD, Department of Radiology, Ren Ji Hospital, School of Medicine, Shanghai Jiao Tong University, Shanghai, China).

tissues, as well as maintain the signal contribution from T_2 that further differentiates these tissues (206). A case report by Rodríguez-Soto et al. demonstrated the ability of RSI to isolate different water pools in the breast by significantly increasing lesion conspicuity in a lactating woman (high BPE) with biopsy proven IDC compared to both DCE-MRI and conventional DWI (207). Thus, emphasizing the utility of the technique in identifying active disease separate from edema from a lactating breast. Studies of RSI in the breast have thus been performed in patients with known malignancy, and like other diffusion techniques may be challenged in evaluating small lesions. Next steps include adapting RSI to high resolution diffusion imaging, thus allowing the technique to be useful in a screening population (208)

Time Dependent Diffusion (TDD)

While ADC values obtained from conventional DWI reflect tissue cellularity, it cannot specifically differentiate underlying sub-cellular parameters such as cell size or density (209). Time dependent diffusion, sometimes called temporal diffusion spectroscopy, has shown potential as an emerging parameter to provide added information about the intracellular space, and thereby further characterize tissue biology (209).

Lima et al. demonstrated the time dependence of the ADC value in breast cancer xenografts, with increasing ADC values with increasing diffusion time (210). A few geometric models applied to the diffusion weighted signal, some of which utilize oscillating gradient spin echo (OGSE) acquisitions in addition to pulsed gradient spin echo (PGSE), quantified intracellular diffusion restriction and provided adequate estimates of cell size and intracellular volume (209, 211).

Teruel et al. applied a stimulated echo acquisition mode (STEAM) with multiple diffusion times to normal and pathologic breasts and used a DTI model to fit the data (**Figure 10**). Results showed differences in the estimation of the radial diameter and diffusion length scales for healthy fibroglandular tissue, a simple cyst, and malignant lesions. Complete fat suppression was also seen with longer diffusion times, allowing for more accurate T1 mapping (212).

A few groups have shown that TDD methods increase lesion contrast and may play a role in assessment of treatment response by detecting changes in cell size (211, 213–215). More research is needed to fully understand the application of TDD In breast cancer.

Radiomics

With the growth of precision medicine comes an opportunity for radiologists to add value by providing relevant information about the patient's underlying disease in a non-invasive manner. Radiomics is a method of extracting and analyzing large amounts of advanced quantitative data to create a mineable database (216, 217). This data is then used to create analytic and predictive models to correlate radiomic features with diagnostic and prognostic information. Ideally, these radiomic features or signatures would provide insight to the underlying tumor biology and contribute to individualized treatment (216). The standard radiomic process includes 1) image acquisition and reconstruction, 2) image segmentation 3) feature extraction and qualification, and 4) database creation (216, 217).

Ye et al. provided an in depth review of the application of radiomics in breast MRI (216). Although most of the studies were based on DCE modalities, a few were multiparametric and included DWI acquisitions, and even fewer utilized only DWI. For this review, only studies that included DW images will be discussed.

A few groups have evaluated the ability of radiomic models to characterize breast lesions.

Bickelhaupt et al. reported that a Radiomics model based on DKI in the evaluation of mammographic BI-RADS 4 and 5 lesions outperformed ADC and K alone, with improved specificity and a reduction in the number of false positive results by 70% (218). A few multiparametric studies have also demonstrated the ability of radiomic models to differentiate benign from malignant lesions (219–221). Zhang et al. demonstrated an AUC of 0.921 and accuracy of 0.833 in discriminating lesions when using a model based off of T2 weighted, DKI, and quantitative DCE-MRI parameter maps (221). Parekh and Jacobs presented a new radiomic feature mapping framework created from multiple MR

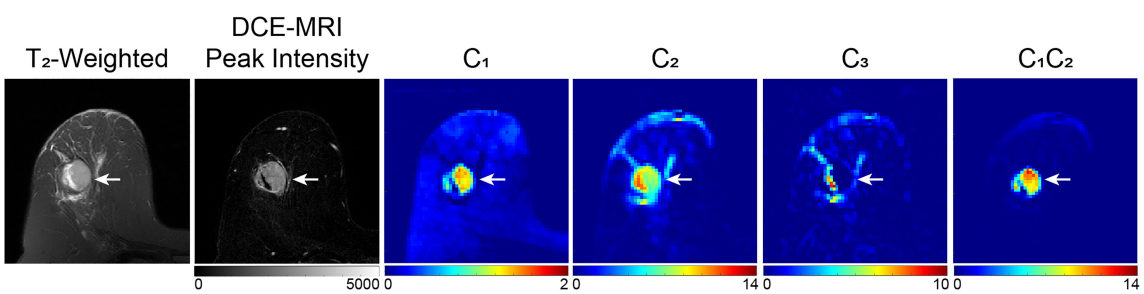

FIGURE 9 | Example of three-compartment RSI analysis in a 49-year-old patient with invasive ductal carcinoma. C_1, C_2, and C_3 maps correspond to the slowest, intermediary, and fastest diffusion compartments, respectively. The lesion, indicated by the white arrow, is hypointense on C_1 and C_2 maps compared to surrounding healthy tissue, whereas there is little difference in the C_3 compartment, which is suggested to correspond to vasculature. The product of C_1 and C_2 (C_1C_2) results in the greatest tumor conspicuity. DWI images were acquired at b = 0, 500, 1500, and 4000 s/mm^2 on a 3T scanner, with 50% reduced FOV and without parallel imaging (206).

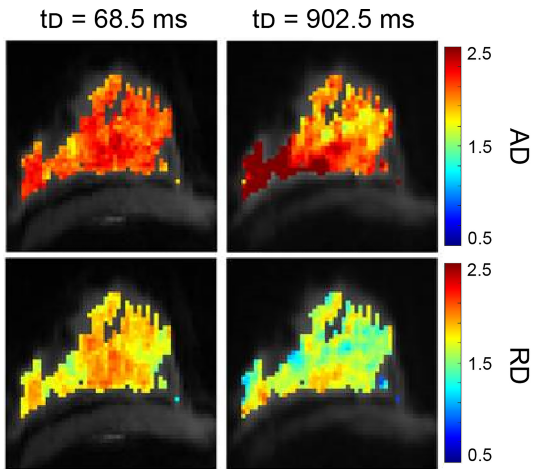

FIGURE 10 | Example of STEAM analysis in a healthy volunteer. The protocol collected a prototype STEAM-DTI sequence with two b-values (0, 500 s/mm^2) in six directions with parallel imaging in a 3T scanner. Axial diffusivity (AD, first row) and radial diffusivity (RD, second row) [μm^2/ms] parametric maps at the shortest and longest diffusion time for healthy fibroglandular tissue are shown (212). (Courtesy of Jose Teruel, PhD, Department of Radiation Oncology, NYU Langone Medical Center, New York, New York, USA).

sequences and evaluated the utility of this method in the characterization of breast lesions. Authors reported significant differences in textural features between malignant and benign lesions, with an overall sensitivity and specificity of 93% and 85%. Radiomic feature maps provide the added benefit of visual interpretation of feature values as well as lesion heterogeneity (222).

Recent studies have also evaluated the role of radiomics in the prediction of breast cancer subtypes and other prognostic factors. Holli-Helenius et al. reported that the texture features sum entropy and sum variance significantly differed between Luminal A and Luminal B subtypes, with a AUC of 0.876 for the combined radiomic model (223). Other studies have also demonstrated the potential of texture analysis to discriminate among different breast cancer subtypes (224–226). A study by Leithner et al. showed improved accuracy for breast cancer subtype classification when segmentation was performed on the ADC maps, with the highest discriminatory ability seen with Luminal B and HER2 enriched subtypes (227).

In a study by Dong et al., a radiomic model derived from a combination of T2-FS and DWI textural features demonstrated high performance in the prediction of axillary lymph node metastases, with an AUC of 0.863 in the training set and 0.805 in the validation set (228). Another group created predictive models from T1WI, T2WI, DWI and the second post-contrast phase of DCE sequences, and reported an AUC of 0.85 for DWI alone in the prediction of axillary lymph node metastases (229). The highest performance was reported for the model based off of CE2 images with kinetic features, with an AUC of 0.91 (229). No additional performance benefit was found when features from all four sequences were combined, suggesting that DWI radiomic signatures may not play as important a role in the preoperative prediction of axillary lymph node metastases (229).

A few groups have also shown good performance in the ability of radiomic models to predict Ki-67 expression (AUC 0.7 – 0.888) (230–232). A study by Fan et al. found that radiomic analysis of "super resolution" (SR) ADC images better predicted histologic grade and Ki-67 expression compared to features based on conventional ADC images, demonstrating the potential added diagnostic value of a SR technique (233).

The degree to which DWI-based radiomic analyses can predict response to NAC has been investigated by a few groups. Liu et al. found that a radiomics model derived from multiparametric MRI and clinical information better predicted pCR to NAC than individual clinical models and radiomic signatures (234). A model built from pretreatment texture and kinetic parameters significantly helped predict nonresponders with 84% sensitivity in another study (235). A study by Panzeri et al., however, reported no significant correlations between ADC texture radiomic signatures and response to NAC, but parameters derived from DCE-MRI showed utility in predicting response (236).

Comparison across studies is limited as the methods and population sizes used to develop radiomic signatures vary. The role of DWI in radiomics remains under active investigation, many groups demonstrated the potential to aid in the diagnosis, prognosis and surveillance of breast cancer.

Ultra-High Field Strength

Increasing the field strength is another method in which diffusion-weighted imaging may be improved. The increased CNR and SNR at higher field strengths lead to improved spatial and temporal resolution, which may increase lesion conspicuity and detection. A meta-analysis by Shi et al. included 61 studies comprising 5205 breast lesions and found no significant difference in the diagnostic performance of DWI in the differentiation of malignant and benign lesions at 1.5 T compared to 3 T (32).

Several technical limitations arise when increasing the field strength, particularly at ultra-high fields (7T and above). At 7T, DWI must overcome limitations due to the increased specific absorption rate (SAR) in addition to heterogeneous fat suppression and T2* blurring, which degrade image quality. A few groups have mitigated these issues through the use of bilateral coil designs and demonstrated the feasibility of DWI of the breast at 7T (**Figure 11**) (26, 237–240).

Bogner et al. showed that combination of rs-EPI DWI with parallel imaging at 7T significantly reduced artifacts and improved image quality, with submillimeter resolution and good diagnostic performance in the characterization of breast lesions (238). A study by Gruber et al. compared DWI of breast lesions at 7T versus 3T using rs-EPI and found increased sensitivity (100% compared to 94%) at 7T for the same ADC threshold and specificity, comparable SNR and CNR, and a 2.4 times higher spatial resolution. These findings suggest that 7T may aid in the detection of smaller lesions that otherwise are more difficult to visualize (239).

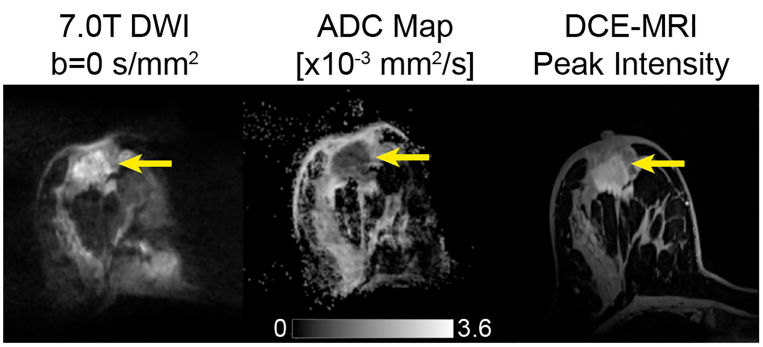

FIGURE 11 | 39-year-old female with invasive ductal carcinoma, imaged at 7T using a dedicated four-channel double-tuned $^{31}P/^{1}H$ breast coil. Images shown are b=0 s/mm^2, corresponding ADC map, and DCE-MRI peak intensity subtraction. The mean ADC of the tumor shown is 0.71 ± 0.18 × 10^{-3} mm^2/s. For DWI, a transverse DWI read-out segmented echo-planar imaging sequence was used. For DCE, patients were intravenously injected with a single dose of contrast agent (gadoterate meglumine) as a bolus, followed by a 20-mL saline flush after three of the 18 repetitions of the time-resolved angiographic imaging with stochastic trajectories sequence (26). (Courtesy of Katja Pinker-Domenig, MD, PhD, Department of Radiology, Memorial Sloan Kettering Cancer Center, New York, New York, USA).

Multiparametric MRI of the breast at 7T was also performed by a few groups (26, 237, 240). Of note, Pinker et al. generated excellent quality images and found that multiparametric MR eliminated false negative findings and decreased the number of false positive findings in 40 women (26). Clinically, this may translate into a reduced number of unnecessary biopsies and improved diagnostic accuracy.

Though most of the literature consists of a few studies with small sample sizes, the results are promising with the main limitation being the general lack of accessibility to 7T scanners for most patients (and breast imaging researchers).

DISCUSSION

An abundance of evidence has shown the utility of DWI as an imaging biomarker for breast cancer, with applications ranging from screening, lesion detection and characterization, and treatment response evaluation. The monoexponential ADC has shown promise in differentiating benign and malignant lesions; however, significant overlap in reported ADC ranges for these tissues limit the clinical utility of ADC cutoffs. Further, there have been conflicting results in the ability of ADC in discriminating lesion subtypes, likely owing to varying study design and protocol differences. Recently, the ACRIN 6698 trial showed high precision in a multi-institution and multi-platform setting, marking a milestone in the validation of DWI as a biomarker in breast imaging and highlighting the need for standardized protocols. As a result, a breast section was incorporated into the 2019 QIBA profile, providing guidance for implementation in community practice.

As described throughout this review, some advanced DWI models require data acquisition at high b-values, which increases susceptibility to B_0 inhomogeneity-induced artifacts and noise, especially for EPI-based sequences. Thus, several methods have been proposed to address this issue, but are beyond the scope of this review (241). An additional limitation of breast DWI is that due to the breast's underlying tissue complexity (e.g. intricate composition of fat, fibroglandular tissue and cancers), measurements of DWI-derived parameters in tissues different from fat tend to be underestimated unless adequate fat suppression is achieved (182). Moreover, the monoexponential ADC, which assumes Gaussian diffusion, may not completely capture the complex diffusivity properties of the breast, especially in lesions which display increased tissue heterogeneity. This may explain the conflicting results observed across multiple studies.

To circumvent the limitations of standard ADC, advanced diffusion modeling techniques such as DKI, DTI, IVIM, and RSI may provide added information on the underlying microenvironment by characterizing the non-Gaussian diffusion within tissues. Although promising, the advanced modeling techniques discussed in this paper require further validation through multi-institution studies, optimization of protocol parameters, and demonstration of repeatability and reproducibility prior to use in clinical practice.

With continued research on methods to improve standard DWI, such as increasing field strength and alternative acquisition techniques, advanced modelling techniques, and radiomics, DWI may play an increasingly important role in the evaluation of breast cancer.

AUTHOR CONTRIBUTIONS

AM: this author was responsible for interpreting the relevant literature and drafting the majority of the review. LF: this author was responsible for revising portions of the review and creating the figures. CM: this author was responsible for drafting and revising portions of the review. SB: this author was responsible for revising portions of the review. SL: this author was responsible for generating data and creating figures. AR-S: this author was responsible for critically revising the review and serving as an expert in the field. RR-P: this author was responsible for critically

revising the review, serving as an expert in the field, and approving the final draft. All authors contributed to the article and approved the submitted version.

FUNDING

This work was supported by the California Breast Cancer Research Program [24IB-0056 IDEA Award] and the Krueger v. Wyeth Research Award, and the National Cancer Institute R37 CA249659, and GE Research. The funder was not involved in the study design, collection, analysis, interpretation of data, the writing of this article or the decision to submit it for publication.

ACKNOWLEDGMENTS

We would like to thank our colleagues cited above who contributed images to our review and Alexandra Schlein, our lab manager, for her efforts on this project.

REFERENCES

1. Lehman CD, Schnall MD. Imaging in Breast Cancer: Magnetic Resonance Imaging. *Breast Cancer Res* (2005) 7(5):215. doi: 10.1186/bcr1309
2. Kaiser WA, Zeitler E. MR Imaging of the Breast: Fast Imaging Sequences With and Without Gd-DTPA. Preliminary Observations. *Radiology* (1989) 170(3 Pt 1):681–6. doi: 10.1148/radiology.170.3.2916021
3. Heywang SH, Fenzl G, Hahn D, Krischke I, Edmaier M, Eiermann W, et al. MR Imaging of the Breast: Comparison With Mammography and Ultrasound. *J Comput Assist Tomogr.* (1986) 10(4):615–20. doi: 10.1097/00004728-198607000-00014
4. Aminololama-Shakeri S, Lewin J, Appelton C, Lee CS, Giess CS, Ojeda-Fournier H, et al. *ACR Practice Parameter for the Performance of Contrast-Enhanced Magnetic Resonance Imaging (MRI) of the Breast*. American College of Radiology (2021). Available at: https://www.acr.org/-/media/ACR/Files/Practice-Parameters/mr-guided-breast.pdf?la=en.
5. White NS, McDonald C, Farid N, Kuperman J, Karow D, Schenker-Ahmed NM, et al. Diffusion-Weighted Imaging in Cancer: Physical Foundations and Applications of Restriction Spectrum Imaging. *Cancer Res* (2014) 74 (17):4638–52. doi: 10.1158/0008-5472.CAN-13-3534
6. Camps-Herrero J. Diffusion-Weighted Imaging of the Breast: Current Status as an Imaging Biomarker and Future Role. *BJR|Open* (2019) 1(1):20180049. doi: 10.1259/bjro.20180049
7. Basser PJ. Inferring Microstructural Features and the Physiological State of Tissues From Diffusion-Weighted Images. *NMR BioMed* (1995) 8(7–8):333–44. doi: 10.1002/nbm.1940080707
8. Basser PJ, Pierpaoli C. Microstructural and Physiological Features of Tissues Elucidated by Quantitative-Diffusion-Tensor MRI. *J Magn Reson B* (1996) 111(3):209–19. doi: 10.1006/jmrb.1996.0086
9. Partridge SC, McDonald ES. Diffusion Weighted MRI of the Breast: Protocol Optimization, Guidelines for Interpretation, and Potential Clinical Applications. *Magn Reson Imaging Clin N Am* (2013) 21(3):601–24. doi: 10.1016/j.mric.2013.04.007
10. Amornsiripanitch N, Bickelhaupt S, Shin HJ, Dang M, Rahbar H, Pinker K, et al. Diffusion-Weighted MRI for Unenhanced Breast Cancer Screening. *Radiology* (2019) 293(3):504–20. doi: 10.1148/radiol.2019182789
11. Monticciolo DL, Newell MS, Moy L, Niell B, Monsees B, Sickles EA. Breast Cancer Screening in Women at Higher-Than-Average Risk: Recommendations From the ACR. *J Am Coll Radiol* (2018) 15(3 Pt A):408–14. doi: 10.1016/j.jacr.2017.11.034
12. McDonald ES, Hammersley JA, Chou S-HS, Rahbar H, Scheel JR, Lee CI, et al. Performance of DWI as a Rapid Unenhanced Technique for Detecting Mammographically Occult Breast Cancer in Elevated-Risk Women With Dense Breasts. *Am J Roentgenol* (2016) 207(1):205–16. doi: 10.2214/AJR.15.15873
13. Yabuuchi H, Matsuo Y, Sunami S, Kamitani T, Kawanami S, Setoguchi T, et al. Detection of non-Palpable Breast Cancer in Asymptomatic Women by Using Unenhanced Diffusion-Weighted and T2-Weighted MR Imaging: Comparison With Mammography and Dynamic Contrast-Enhanced MR Imaging. *Eur Radiol* (2011) 21(1):11–7. doi: 10.1007/s00330-010-1890-8
14. Amornsiripanitch N, Rahbar H, Kitsch AE, Lam DL, Weitzel B, Partridge SC. Visibility of Mammographically Occult Breast Cancer on Diffusion-Weighted MRI Versus Ultrasound. *Clin Imaging* (2018) 49:37–43. doi: 10.1016/j.clinimag.2017.10.017
15. Pinker K, Moy L, Sutton EJ, Mann RM, Weber M, Thakur SB, et al. Diffusion-Weighted Imaging With Apparent Diffusion Coefficient Mapping for Breast Cancer Detection as a Stand-Alone-Parameter: Comparison With Dynamic Contrast-Enhanced and Multiparametric Magnetic Resonance Imaging. *Invest Radiol* (2018) 53(10):587–95. doi: 10.1097/RLI.0000000000000465
16. Baltzer P, Mann RM, Iima M, Sigmund EE, Clauser P, Gilbert FJ, et al. Diffusion-Weighted Imaging of the Breast-a Consensus and Mission Statement From the EUSOBI International Breast Diffusion-Weighted Imaging Working Group. *Eur Radiol* (2020) 30(3):1436–50. doi: 10.1007/s00330-019-06510-3
17. Geach R, Jones LI, Harding SA, Marshall A, Taylor-Phillips S, McKeown-Keegan S, et al. The Potential Utility of Abbreviated Breast MRI (FAST MRI) as a Tool for Breast Cancer Screening: A Systematic Review and Meta-Analysis. *Clin Radiol* (2021) 76(2):154.e11–154.e22. doi: 10.1016/j.crad.2020.08.032
18. Yamada T, Kanemaki Y, Okamoto S, Nakajima Y. Comparison of Detectability of Breast Cancer by Abbreviated Breast MRI Based on Diffusion-Weighted Images and Postcontrast MRI. *Jpn J Radiol* (2018) 36 (5):331–9. doi: 10.1007/s11604-018-0731-6
19. Baltzer PAT, Benndorf M, Dietzel M, Gajda M, Camara O, Kaiser WA. Sensitivity and Specificity of Unenhanced MR Mammography (DWI Combined With T2-Weighted TSE Imaging, ueMRM) for the Differentiation of Mass Lesions. *Eur Radiol* (2010) 20(5):1101–10. doi: 10.1007/s00330-009-1654-5
20. Bickelhaupt S, Laun FB, Tesdorff J, Lederer W, Daniel H, Stieber A, et al. Fast and Noninvasive Characterization of Suspicious Lesions Detected at Breast Cancer X-Ray Screening: Capability of Diffusion-Weighted MR Imaging With MIPs. *Radiology* (2015) 278(3):689–97. doi: 10.1148/radiol.2015150425
21. Baltzer PAT, Bickel H, Spick C, Wengert G, Woitek R, Kapetas P, et al. Potential of Noncontrast Magnetic Resonance Imaging With Diffusion-Weighted Imaging in Characterization of Breast Lesions: Intraindividual Comparison With Dynamic Contrast-Enhanced Magnetic Resonance Imaging. *Invest Radiol* (2018) 53(4):229–35. doi: 10.1097/RLI.0000000000000433
22. Kang JW, Shin HJ, Shin KC, Chae EY, Choi WJ, Cha JH, et al. Resonance Screening Using Fused Diffusion-Weighted Imaging and Maximum-Intensity Projection in Patients With a Personal History of Breast Cancer: Role of Fused DWI for Postoperative Screening. *Breast Cancer Res Treat* (2017) 165(17):119–28. doi: 10.1007/s10549-017-4322-5
23. Shahid H, Wiedenhoefer JF, Dornbluth C, Otto P, Kist KA. An Overview of Breast MRI. *Appl Radiol* (2016) 45(10):7–13. doi: 10.37549/AR2317
24. Rahbar H, Partridge SC. Multiparametric Breast MRI of Breast Cancer. *Magn Reson Imaging Clin N Am* (2016) 24(1):223–38. doi: 10.1016/j.mric.2015.08.012
25. Zhang L, Tang M, Min Z, Lu J, Lei X, Zhang X. Accuracy of Combined Dynamic Contrast-Enhanced Magnetic Resonance Imaging and Diffusion-Weighted Imaging for Breast Cancer Detection: A Meta-Analysis. *Acta Radiol* (2016) 57(6):651–60. doi: 10.1177/0284185115597265
26. Pinker K, Baltzer P, Bogner W, Leithner D, Trattnig S, Zaric O, et al. Multiparametric MR Imaging With High-Resolution Dynamic Contrast-Enhanced and Diffusion-Weighted Imaging at 7 T Improves the Assessment of Breast Tumors: A Feasibility Study. *Radiology* (2015) 276(2):360–70. doi: 10.1148/radiol.15141905

27. Partridge SC, WB D, BF K, PR E, SW W, Lehman CD. Quantitative Diffusion-Weighted Imaging as an Adjunct to Conventional Breast MRI for Improved Positive Predictive Value. *Am J Roentgenol* (2009) 193 (6):1716–22. doi: 10.2214/AJR.08.2139
28. Khouli RH EI, Jacobs MA, Mezban SD, Huang P, Kamel IR, Macura KJ, et al. Diffusion-Weighted Imaging Improves the Diagnostic Accuracy of Conventional 3.0-T Breast MR Imaging1. *Radiology* (2010) 256(1):64–73. doi: 10.1148/radiol.10091367
29. Baxter GC, Graves MJ, Gilbert FJ, Patterson AJ. A Meta-Analysis of the Diagnostic Performance of Diffusion MRI for Breast Lesion Characterization. *Radiology* (2019) 291(3):632–41. doi: 10.1148/radiol.2019182510
30. Chen X, Li W, Zhang Y, Wu Q, Guo Y, Bai Z. Meta-Analysis of Quantitative Diffusion-Weighted MR Imaging in the Differential Diagnosis of Breast Lesions. *BMC Cancer* (2010) 10(1):693. doi: 10.1186/1471-2407-10-693
31. Tsushima Y, Takahashi-Taketomi A, Endo K. Magnetic Resonance (MR) Differential Diagnosis of Breast Tumors Using Apparent Diffusion Coefficient (ADC) on 1.5-T. *J Magn Reson Imaging* (2009) 30(2):249–55. doi: 10.1002/jmri.21854
32. Shi R, Yao Q, Wu L, Xu J. Breast Lesions: Diagnosis Using Diffusion Weighted Imaging at 1.5T and 3.0T—Systematic Review and Meta-Analysis. *Clin Breast Cancer* (2018) 18(3):e305–20. doi: 10.1016/j.clbc.2017.06.011
33. Surov A, Meyer HJ, Wienke A. Can Apparent Diffusion Coefficient (ADC) Distinguish Breast Cancer From Benign Breast Findings? A Meta-Analysis Based on 13 847 Lesions. *BMC Cancer* (2019) 19(1):955. doi: 10.1186/s12885-019-6201-4
34. Ding J-R, Wang D-N, Pan J-L. Apparent Diffusion Coefficient Value of Diffusion-Weighted Imaging for Differential Diagnosis of Ductal Carcinoma *in Situ* and Infiltrating Ductal Carcinoma. *J Cancer Res Ther* (2016) 12 (2):744–50. doi: 10.4103/0973-1482.154093
35. Zhao S, Shao G, Chen P, Li L, Yang Y, Zhao X, et al. Diagnostic Performance of Minimum Apparent Diffusion Coefficient Value in Differentiating the Invasive Breast Cancer and Ductal Carcinoma *in Situ*. *J Cancer Res Ther* (2019) 15(4):871–5. doi: 10.4103/jcrt.JCRT_607_18
36. Cho GY, Moy L, Kim SG, Baete SH, Moccaldi M, Babb JS, et al. Evaluation of Breast Cancer Using Intravoxel Incoherent Motion (IVIM) Histogram Analysis: Comparison With Malignant Status, Histological Subtype, and Molecular Prognostic Factors. *Eur Radiol* (2016) 26(8):2547–58. doi: 10.1007/s00330-015-4087-3
37. Horvat JV, Bernard-Davila B, Helbich TH, Zhang M, Morris EA, Thakur SB, et al. Diffusion-Weighted Imaging (DWI) With Apparent Diffusion Coefficient (ADC) Mapping as a Quantitative Imaging Biomarker for Prediction of Immunohistochemical Receptor Status, Proliferation Rate, and Molecular Subtypes of Breast Cancer. *J Magn Reson Imaging* (2019) 50(3):836–46. doi: 10.1002/jmri.26697
38. Jatoi I, Hilsenbeck SG, Clark GM, Osborne CK. Significance of Axillary Lymph Node Metastasis in Primary Breast Cancer. *J Clin Oncol* (1999) 17 (8):2334–40. doi: 10.1200/JCO.1999.17.8.2334
39. Sui WF, Chen X, Peng ZK, Ye J, Wu JT. The Diagnosis of Metastatic Axillary Lymph Nodes of Breast Cancer By Diffusion Weighted Imaging: A Meta-Analysis and Systematic Review. *World J Surg Oncol* (2016) 14(1):155. doi: 10.1186/s12957-016-0906-5
40. Kim EJ, Kim SH, Park GE, Kang BJ, Song BJ, Kim YJ, et al. Histogram Analysis of Apparent Diffusion Coefficient at 3.0t: Correlation With Prognostic Factors and Subtypes of Invasive Ductal Carcinoma. *J Magn Reson Imaging* (2015) 42(6):1666–78. doi: 10.1002/jmri.24934
41. Ren C, Zou Y, Zhang X, Li K. Diagnostic Value of Diffusion-Weighted Imaging-Derived Apparent Diffusion Coefficient and its Association With Histological Prognostic Factors in Breast Cancer. *Oncol Lett* (2019) 18 (3):3295–303. doi: 10.3892/ol.2019.10651
42. Belli P, Costantini M, Bufi E, Giardina GG, Rinaldi P, Franceschini G, et al. Diffusion Magnetic Resonance Imaging in Breast Cancer Characterisation: Correlations Between the Apparent Diffusion Coefficient and Major Prognostic Factors. *Radiol Med* (2015) 120(3):268–76. doi: 10.1007/s11547-014-0442-8
43. Surov A, Chang Y-W, Li L, Martincich L, Partridge SC, Kim JY, et al. Apparent Diffusion Coefficient Cannot Predict Molecular Subtype and Lymph Node Metastases in Invasive Breast Cancer: A Multicenter Analysis. *BMC Cancer* (2019) 19(1):1043. doi: 10.1186/s12885-019-6298-5
44. Suo S, Cheng F, Cao M, Kang J, Wang M, Hua J, et al. Multiparametric Diffusion-Weighted Imaging in Breast Lesions: Association With Pathologic Diagnosis and Prognostic Factors. *J Magn Reson Imaging* (2017) 46(3):740–50. doi: 10.1002/jmri.25612
45. Park SH, Choi H-Y, Hahn SY. Correlations Between Apparent Diffusion Coefficient Values of Invasive Ductal Carcinoma and Pathologic Factors on Diffusion-Weighted MRI at 3.0 Tesla. *J Magn Reson Imaging* (2015) 41 (1):175–82. doi: 10.1002/jmri.24519
46. Choi SY, Chang Y-W, Park HJ, Kim HJ, Hong SS, Seo DY. Correlation of the Apparent Diffusion Coefficiency Values on Diffusion-Weighted Imaging With Prognostic Factors for Breast Cancer. *Br J Radiol* (2012) 85(1016): e474–9. doi: 10.1259/bjr/79381464
47. Meng L, Ma P. Apparent Diffusion Coefficient Value Measurements With Diffusion Magnetic Resonance Imaging Correlated With the Expression Levels of Estrogen and Progesterone Receptor in Breast Cancer: A Meta-Analysis. *J Cancer Res Ther* (2016) 12(1):36–42. doi: 10.4103/0973-1482.150418
48. Suo S, Zhang D, Cheng F, Cao M, Hua J, Lu J, et al. Added Value of Mean and Entropy of Apparent Diffusion Coefficient Values for Evaluating Histologic Phenotypes of Invasive Ductal Breast Cancer With MR Imaging. *Eur Radiol* (2019) 29(3):1425–34. doi: 10.1007/s00330-018-5667-9
49. Okuma H, Sudah M, Kettunen T, Niukkanen A, Sutela A, Masarwah A, et al. Peritumor to Tumor Apparent Diffusion Coefficient Ratio is Associated With Biologically More Aggressive Breast Cancer Features and Correlates With the Prognostication Tools. *PloS One* (2020) 15(6):e0235278. doi: 10.1371/journal.pone.0235278
50. Aydin H, Guner B, Esen Bostanci I, Bulut ZM, Aribas BK, Dogan L, et al. Is There Any Relationship Between Adc Values of Diffusion-Weighted Imaging and the Histopathological Prognostic Factors of Invasive Ductal Carcinoma? *Br J Radiol* (2018) 91(1084):20170705. doi: 10.1259/bjr.20170705
51. Martincich L, Deantoni V, Bertotto I, Redana S, Kubatzki F, Sarotto I, et al. Correlations Between Diffusion-Weighted Imaging and Breast Cancer Biomarkers. *Eur Radiol* (2012) 22(7):1519–28. doi: 10.1007/s00330-012-2403-8
52. Kamitani T, Matsuo Y, Yabuuchi H, Fujita N, Nagao M, Jinnouchi M, et al. Correlations Between Apparent Diffusion Coefficient Values and Prognostic Factors of Breast Cancer. *Magn Reson Med Sci* (2013) 12(3):193–9. doi: 10.2463/mrms.2012-0095
53. Tezcan Ş, Uslu N, Öztürk FU, Akçay EY, Tezcaner T. Diffusion-Weighted Imaging of Breast Cancer: Correlation of the Apparent Diffusion Coefficient Value With Pathologic Prognostic Factors. *Eur J Breast Health* (2019) 15 (4):262–7. doi: 10.5152/ejbh.2019.4860
54. Amornsiripanitch N, Nguyen VT, Rahbar H, Hippe D, Gadi VK, Rendi MH, et al. Diffusion-Weighted MRI Characteristics Associated With Prognostic Pathological Factors and Recurrence Risk in Invasive ER+/HER2– Breast Cancers. *J Magn Reson Imaging* (2018) 48(1):226–36. doi: 10.1002/jmri.25909
55. Surov A, Clauser P, Chang Y-W, Li L, Martincich L, Partridge SC, et al. Can Diffusion-Weighted Imaging Predict Tumor Grade and Expression of Ki-67 in Breast Cancer? A Multicenter Analysis. *Breast Cancer Res* (2018) 20(1):58. doi: 10.1186/s13058-018-0991-1
56. Suo S, Cheng F, Cao M, Kang J, Wang M, Hua J, et al. Multiparametric Diffusion-Weighted Imaging in Breast Lesions: Association With Pathologic Diagnosis and Prognostic Factors: DWI in Breast Lesions. *J Magn Reson Imaging* (2017) 46(3):740–50. doi: 10.1002/jmri.25612
57. Goldhirsch A, Wood WC, Coates AS, Gelber RD, Thürlimann B, Senn H-J, et al. Strategies for Subtypes–Dealing With the Diversity of Breast Cancer: Highlights of the St. Gallen International Expert Consensus on the Primary Therapy of Early Breast Cancer 2011. *Ann Oncol: Official J Euro Soc Med Oncol* (2011) 22(8):1736–47. doi: 10.1093/annonc/mdr304
58. Meyer H-J, Wienke A, Surov A. Diffusion Weighted Imaging of Different Breast Cancer Molecular Subtypes. A Systematic Review and Meta Analysis. *Breast Care (Basel)* (2022) 17(1):47–54. doi: 10.1159/000514407
59. Surov A, Meyer HJ, Wienke A. Associations Between Apparent Diffusion Coefficient (ADC) and KI 67 in Different Tumors: A Meta-Analysis. Part 1:

ADCmean. *Oncotarget* (2017) 8(43):75434–44. doi: 10.18632/oncotarget.20406
60. Cheon H, Kim HJ, Kim TH, Ryeom H-K, Lee J, Kim GC, et al. Invasive Breast Cancer: Prognostic Value of Peritumoral Edema Identified at Preoperative MR Imaging. *Radiology* (2018) 287(1):68–75. doi: 10.1148/radiol.2017171157
61. Kettunen T, Okuma H, Auvinen P, Sudah M, Tiainen S, Sutela A, et al. Peritumoral ADC Values in Breast Cancer: Region of Interest Selection, Associations With Hyaluronan Intensity, and Prognostic Significance. *Eur Radiol* (2020) 30(1):38–46. doi: 10.1007/s00330-019-06361-y
62. Panzironi G, Moffa G, Galati F, Marzocca F, Rizzo V, Pediconi F. Peritumoral Edema as a Biomarker of the Aggressiveness of Breast Cancer: Results of a Retrospective Study on a 3 T Scanner. *Breast Cancer Res Treat* (2020) 181(1):53–60. doi: 10.1007/s10549-020-05592-8
63. Thompson AM, Moulder-Thompson SL. Neoadjuvant Treatment of Breast Cancer. *Ann Oncol* (2012) 23:x231–6. doi: 10.1093/annonc/mds324
64. Yeh E, Slanetz P, Kopans DB, Rafferty E, Georgian-Smith D, Moy L, et al. Prospective Comparison of Mammography, Sonography, and MRI in Patients Undergoing Neoadjuvant Chemotherapy for Palpable Breast Cancer. *Am J Roentgenol* (2005) 184(3):868–77. doi: 10.2214/ajr.184.3.01840868
65. Gu Y-L, Pan S-M, Ren J, Yang Z-X, Jiang G-Q. Role of Magnetic Resonance Imaging in Detection of Pathologic Complete Remission in Breast Cancer Patients Treated With Neoadjuvant Chemotherapy: A Meta-Analysis. *Clin Breast Cancer* (2017) 17(4):245–55. doi: 10.1016/j.clbc.2016.12.010
66. Gao W, Guo N, Dong T. Diffusion-Weighted Imaging in Monitoring the Pathological Response to Neoadjuvant Chemotherapy in Patients With Breast Cancer: A Meta-Analysis. *World J Surg Oncol* (2018) 16(1):145. doi: 10.1186/s12957-018-1438-y
67. Chu W, Jin W, Liu D, Wang J, Geng C, Chen L, et al. Diffusion-Weighted Imaging in Identifying Breast Cancer Pathological Response to Neoadjuvant Chemotherapy: A Meta-Analysis. *Oncotarget* (2017) 9(6):7088–100. doi: 10.18632/oncotarget.23195
68. Shin HJ, Baek H-M, Ahn J-H, Baek S, Kim H, Cha JH, et al. Prediction of Pathologic Response to Neoadjuvant Chemotherapy in Patients With Breast Cancer Using Diffusion-Weighted Imaging and MRS. *NMR Biomed* (2012) 25(12):1349–59. doi: 10.1002/nbm.2807
69. Li X, Cheng L, Liu M, Zhang Y, Wang J, Zhang A, et al. DW-MRI ADC Values can Predict Treatment Response in Patients With Locally Advanced Breast Cancer Undergoing Neoadjuvant Chemotherapy. *Med Oncol* (2012) 29(2):425–31. doi: 10.1007/s12032-011-9842-y
70. Bedair R, Priest AN, Patterson AJ, McLean MA, Graves MJ, Manavaki R, et al. Assessment of Early Treatment Response to Neoadjuvant Chemotherapy in Breast Cancer Using non-Mono-Exponential Diffusion Models: A Feasibility Study Comparing the Baseline and Mid-Treatment MRI Examinations. *Eur Radiol* (2017) 27(7):2726–36. doi: 10.1007/s00330-016-4630-x
71. Woodhams R, Kakita S, Hata H, Iwabuchi K, Kuranami M, Gautam S, et al. Identification of Residual Breast Carcinoma Following Neoadjuvant Chemotherapy: Diffusion-Weighted Imaging—Comparison With Contrast-Enhanced MR Imaging and Pathologic Findings. *Radiology* (2010) 254(2):357–66. doi: 10.1148/radiol.2542090405
72. Fangberget A, Nilsen LB, Hole KH, Holmen MM, Engebraaten O, Naume B, et al. Neoadjuvant Chemotherapy in Breast Cancer-Response Evaluation and Prediction of Response to Treatment Using Dynamic Contrast-Enhanced and Diffusion-Weighted MR Imaging. *Eur Radiol* (2011) 21(6):1188–99. doi: 10.1007/s00330-010-2020-3
73. Bufi E, Belli P, Costantini M, Cipriani A, Di Matteo M, Bonatesta A, et al. Role of the Apparent Diffusion Coefficient in the Prediction of Response to Neoadjuvant Chemotherapy in Patients With Locally Advanced Breast Cancer. *Clin Breast Cancer* (2015) 15(5):370–80. doi: 10.1016/j.clbc.2015.02.002
74. Partridge SC, Zhang Z, Newitt DC, Gibbs JE, Chenevert TL, Rosen MA, et al. Diffusion-Weighted MRI Findings Predict Pathologic Response in Neoadjuvant Treatment of Breast Cancer: The ACRIN 6698 Multicenter Trial. *Radiology* (2018) 289(3):618–27. doi: 10.1148/radiol.2018180273
75. Richard R, Thomassin I, Chapellier M, Scemama A, de Cremoux P, Varna M, et al. Diffusion-Weighted MRI in Pretreatment Prediction of Response to Neoadjuvant Chemotherapy in Patients With Breast Cancer. *Eur Radiol* (2013) 23(9):2420–31. doi: 10.1007/s00330-013-2850-x
76. Agarwal K, Sharma U, Sah RG, Mathur S, Hari S, Seenu V, et al. Pre-Operative Assessment of Residual Disease in Locally Advanced Breast Cancer Patients: A Sequential Study by Quantitative Diffusion Weighted MRI as a Function of Therapy. *Magn Reson Imaging* (2017) 42:88–94. doi: 10.1016/j.mri.2017.06.002
77. Sharma U, Danishad KKA, Seenu V, Jagannathan NR. Longitudinal Study of the Assessment by MRI and Diffusion-Weighted Imaging of Tumor Response in Patients With Locally Advanced Breast Cancer Undergoing Neoadjuvant Chemotherapy. *NMR BioMed* (2009) 22(1):104–13. doi: 10.1002/nbm.1245
78. Shukla-Dave A, Obuchowski NA, Chenevert TL, Jambawalikar S, Schwartz LH, Malyarenko D, et al. Quantitative Imaging Biomarkers Alliance (QIBA) Recommendations for Improved Precision of DWI and DCE-MRI Derived Biomarkers in Multicenter Oncology Trials. *J Magn Reson Imaging* (2019) 49(7):e101–21. doi: 10.1002/jmri.26518
79. Sorace AG, Wu C, Barnes SL, Jarrett AM, Avery S, Patt D, et al. Repeatability, Reproducibility, and Accuracy of Quantitative MRI of the Breast in the Community Radiology Setting. *J Magn Reson Imaging* (2018) 48(3):695–707. doi: 10.1002/jmri.26011
80. Giannotti E, Waugh S, Priba L, Davis Z, Crowe E, Vinnicombe S. Assessment and Quantification of Sources of Variability in Breast Apparent Diffusion Coefficient (ADC) Measurements at Diffusion Weighted Imaging. *Eur J Radiol* (2015) 84(9):1729–36. doi: 10.1016/j.ejrad.2015.05.032
81. Jang M, Kim SM, Yun BL, Ahn HS, Kim SY, Kang E, et al. Reproducibility of Apparent Diffusion Coefficient Measurements in Malignant Breast Masses. *J Korean Med Sci* (2015) 30(11):1689–97. doi: 10.3346/jkms.2015.30.11.1689
82. O'Flynn EAM, Morgan VA, Giles SL, deSouza NM. Diffusion Weighted Imaging of the Normal Breast: Reproducibility of Apparent Diffusion Coefficient Measurements and Variation With Menstrual Cycle and Menopausal Status. *Eur Radiol* (2012) 22(7):1512–8. doi: 10.1007/s00330-012-2399-0
83. Spick C, Bickel H, Pinker K, Bernathova M, Kapetas P, Woitek R, et al. Diffusion-Weighted MRI of Breast Lesions: A Prospective Clinical Investigation of the Quantitative Imaging Biomarker Characteristics of Reproducibility, Repeatability, and Diagnostic Accuracy. *NMR BioMed* (2016) 29(10):1445–53. doi: 10.1002/nbm.3596
84. Newitt DC, Zhang Z, Gibbs JE, Partridge SC, Chenevert TL, Rosen MA, et al. Test-Retest Repeatability and Reproducibility of ADC Measures by Breast DWI: Results From the ACRIN 6698 Trial. *J Magn Reson Imaging* (2019) 49(6):1617–28. doi: 10.1002/jmri.26539
85. QIBA MR Biomarker Committee. MR Diffusion-Weighted Imaging (DWI). In: *Quantitative Imaging Biomarkers Alliance (RSNA)* (2019). Available at: http://qibawiki.rsna.org/images/6/63/QIBA_DWIProfile_Consensus_Dec2019_Final.pdf.
86. de Figueiredo EHMSG, Borgonovi AFNG, Doring TM. Basic Concepts of MR Imaging, Diffusion MR Imaging, and Diffusion Tensor Imaging. *Magn Reson Imaging Clin N Am* (2011) 19(1):1–22. doi: 10.1016/j.mric.2010.10.005
87. An YY, Kim SH, Kang BJ. Differentiation of Malignant and Benign Breast Lesions: Added Value of the Qualitative Analysis of Breast Lesions on Diffusion-Weighted Imaging (DWI) Using Readout-Segmented Echo-Planar Imaging at 3.0 T. *PloS One* (2017) 12(3):e0174681. doi: 10.1371/journal.pone.0174681
88. Wisner DJ, Rogers N, Deshpande VS, Newitt DN, Laub GA, Porter DA, et al. High-Resolution Diffusion-Weighted Imaging for the Separation of Benign From Malignant BI-RADS 4/5 Lesions Found on Breast MRI at 3T. *J Magn Reson Imaging* (2014) 40(3):674–81. doi: 10.1002/jmri.24416
89. Kim YJ, Kim SH, Kang BJ, Park CS, Kim HS, Son YH, et al. Readout-Segmented Echo-Planar Imaging in Diffusion-Weighted MR Imaging in Breast Cancer: Comparison With Single-Shot Echo-Planar Imaging in Image Quality. *Korean J Radiol* (2014) 15(4):403–10. doi: 10.3348/kjr.2014.15.4.403
90. Kanao S, Kataoka M, Iima M, Ohno A, Sakaguchi R, Ohashi A, et al. High-Resolution Diffusion-Weighted MRI of the Breast Using Readout-Segmented EPI and Single-Shot EPI. *Imaging Med* (2017) 9(6):185–90. doi: 10.1002/jmri.24416

91. Bogner W, Pinker-Domenig K, Bickel H, Chmelik M, Weber M, Helbich TH, et al. Readout-Segmented Echo-Planar Imaging Improves the Diagnostic Performance of Diffusion-Weighted MR Breast Examinations at 3.0 T. *Radiology* (2012) 263(1):64–76. doi: 10.1148/radiol.12111494
92. Kishimoto AO, Kataoka M, Iima M, Honda M, Miyake KK, Ohashi A, et al. The Comparison of High-Resolution Diffusion Weighted Imaging (DWI) With High-Resolution Contrast-Enhanced MRI in the Evaluation of Breast Cancers. *Magn Reson Imaging* (2020) 71:161–9. doi: 10.1016/j.mri.2020.03.007
93. Ohlmeyer S, Laun FB, Palm T, Janka R, Weiland E, Uder M, et al. Simultaneous Multislice Echo Planar Imaging for Accelerated Diffusion-Weighted Imaging of Malignant and Benign Breast Lesions. *Invest Radiol* (2019) 54(8):524–30. doi: 10.1097/RLI.0000000000000560
94. Filli L, Ghafoor S, Kenkel D, Liu W, Weiland E, Andreisek G, et al. Simultaneous Multi-Slice Readout-Segmented Echo Planar Imaging for Accelerated Diffusion-Weighted Imaging of the Breast. *Eur J Radiol* (2016) 85(1):274–8. doi: 10.1016/j.ejrad.2015.10.009
95. Song SE, Woo OH, Cho KR, Seo BK, Son YH, Grimm R, et al. Simultaneous Multislice Readout-Segmented Echo Planar Imaging for Diffusion-Weighted MRI in Patients With Invasive Breast Cancers. *J Magn Reson Imaging* (2021) 53(4):1108–15. doi: 10.1002/jmri.27433
96. McKay JA, Church AL, Rubin N, Emory TH, Hoven NF, Kuehn-Hajder JE, et al. A Comparison of Methods for High-Spatial-Resolution Diffusion-Weighted Imaging in Breast MRI. *Radiology* (2020) 297(2):304–12. doi: 10.1148/radiol.2020200221
97. Hu Y, Zhan C, Yang Z, Zhang X, Zhang H, Liu W, et al. Accelerating Acquisition of Readout-Segmented Echo Planar Imaging With a Simultaneous Multi-Slice (SMS) Technique for Diagnosing Breast Lesions. *Eur Radiol* (2021) 31(5):2667–76. doi: 10.1007/s00330-020-07393-5
98. Machida Y, Nomura K, Shimauchi A, Kato Y, Nagatsuka M, Fukuma E. Diffusion-Weighted Imaging With Simultaneous Multi-Slice Echo-Planar Technique for the Diagnosis of Breast Magnetic Resonance Imaging. *Jpn J Radiol* (2020) 38(4):358–64. doi: 10.1007/s11604-020-00919-3
99. Yuan J, Zhao T-C, Tang Y, Panych LP. Reduced Field-of-View Single-Shot Fast Spin Echo Imaging Using Two-Dimensional Spatially Selective Radiofrequency Pulses. *J Magn Reson Imaging* (2010) 32(1):242–8. doi: 10.1002/jmri.22204
100. Rodríguez-Soto AE, Fang LK, Holland D, Zou J, Park HH, Keenan KE, et al. Correction of Artifacts Induced by B0 Inhomogeneities in Breast MRI Using Reduced-Field-Of-View Echo-Planar Imaging and Enhanced Reversed Polarity Gradient Method. *J Magn Reson Imaging* (2021) 53(5):1581–91. doi: 10.1002/jmri.27566
101. Dong H, Li Y, Li H, Wang B, Hu B. Study of the Reduced Field-of-View Diffusion-Weighted Imaging of the Breast. *Clin Breast Cancer* (2014) 14 (4):265–71. doi: 10.1016/j.clbc.2013.12.001
102. Barentsz MW, Taviani V, Chang JM, Ikeda DM, Miyake KK, Banerjee S, et al. Assessment of Tumor Morphology on Diffusion-Weighted (DWI) Breast MRI: Diagnostic Value of Reduced Field of View DWI. *J Magn Reson Imaging* (2015) 42(6):1656–65. doi: 10.1002/jmri.24929
103. Dong H, Li Y, Yu K, Li H. Comparison of Image Quality and Application Values on Different Field-of-View Diffusion-Weighted Imaging of Breast Cancer. *Acta Radiol* (2016) 57(1):19–24. doi: 10.1177/0284185115569106
104. Singer L, Wilmes LJ, Saritas EU, Shankaranarayanan A, Proctor E, Wisner DJ, et al. High-Resolution Diffusion-Weighted Magnetic Resonance Imaging in Patients With Locally Advanced Breast Cancer. *Acad Radiol* (2012) 19 (5):526–34. doi: 10.1016/j.acra.2011.11.003
105. Lee SH, Shin HJ, Moon WK. Diffusion-Weighted Magnetic Resonance Imaging of the Breast: Standardization of Image Acquisition and Interpretation. *Korean J Radiol* (2021) 22(1):9–22. doi: 10.3348/kjr.2020.0093
106. Taviani V, Alley MT, Banerjee S, Nishimura DG, Daniel BL, Vasanawala SS, et al. High-Resolution Diffusion-Weighted Imaging of the Breast With Multiband 2D Radiofrequency Pulses and a Generalized Parallel Imaging Reconstruction. *Magn Reson Med* (2017) 77(1):209–20. doi: 10.1002/mrm.26110
107. McNab JA, Miller KL. Steady-State Diffusion-Weighted Imaging: Theory, Acquisition and Analysis. *NMR BioMed* (2010) 23(7):781–93. doi: 10.1002/nbm.1509
108. Granlund KL, Staroswiecki E, Alley MT, Daniel BL, Hargreaves BA. High-Resolution, Three-Dimensional Diffusion-Weighted Breast Imaging Using DESS. *Magn Reson Imaging* (2014) 32(4):330–41. doi: 10.1016/j.mri.2013.12.014
109. Moran CJ, Cheng JY, Sandino CM, Carl M, Alley MT, Rosenberg J, et al. Diffusion-Weighted Double-Echo Steady-State With a Three-Dimensional Cones Trajectory for non-Contrast-Enhanced Breast MRI. *J Magn Reson Imaging* (2021) 53(5):1594–605. doi: 10.1002/jmri.27492
110. Tendler BC, Foxley S, Cottaar M, Jbabdi S, Miller KL. Modeling an Equivalent B-Value in Diffusion-Weighted Steady-State Free Precession. *Magn Reson Med* (2020) 84(2):873–84. doi: 10.1002/mrm.28169
111. Daniel BL, Granlund KL, Moran CJ, Alley MT, Lipson J, Ikeda DM, et al. Breast MRI Without Gadolinium: Utility of 3D DESS, a New 3D Diffusion Weighted Gradient-Echo Sequence. *Eur J Radiol* (2012) 81 Suppl 1:S24–26. doi: 10.1016/S0720-048X(12)70010-4
112. Han X, Li J, Wang X. Comparison and Optimization of 3.0 T Breast Images Quality of Diffusion-Weighted Imaging With Multiple B-Values. *Acad Radiol* (2017) 24(4):418–25. doi: 10.1016/j.acra.2016.11.006
113. Peters NHGM, Vincken KL, van den Bosch MAAJ, Luijten PR, Mali WPTM, Bartels LW. Quantitative Diffusion Weighted Imaging for Differentiation of Benign and Malignant Breast Lesions: The Influence of the Choice of B-Values. *J Magn Reson Imaging* (2010) 31(5):1100–5. doi: 10.1002/jmri.22152
114. Pereira FPA, Martins G, Figueiredo E, Domingues MNA, Domingues RC, da Fonseca LMB, et al. Assessment of Breast Lesions With Diffusion-Weighted MRI: Comparing the Use of Different B Values. *AJR Am J Roentgenol* (2009) 193(4):1030–5. doi: 10.2214/AJR.09.2522
115. Bogner W, Gruber S, Pinker K, Grabner G, Stadlbauer A, Weber M, et al. Diffusion-Weighted MR for Differentiation of Breast Lesions at 3.0 T: How Does Selection of Diffusion Protocols Affect Diagnosis? *Radiology* (2009) 253 (2):341–51. doi: 10.1148/radiol.2532081718
116. Bickel H, Pinker K, Polanec S, Magometschnigg H, Wengert G, Spick C, et al. Diffusion-Weighted Imaging of Breast Lesions: Region-Of-Interest Placement and Different ADC Parameters Influence Apparent Diffusion Coefficient Values. *Eur Radiol* (2017) 27(5):1883–92. doi: 10.1007/s00330-016-4564-3
117. Gity M, Moradi B, Arami R, Arabkheradmand A, Kazemi MA. Two Different Methods of Region-Of-Interest Placement for Differentiation of Benign and Malignant Breast Lesions by Apparent Diffusion Coefficient Value. *Asian Pac J Cancer Prev* (2018) 19(10):2765–70. doi: 10.22034/APJCP.2018.19.10.2765
118. Nogueira L, Brandão S, Matos E, Nunes RG, Ferreira HA, Loureiro J, et al. Region of Interest Demarcation for Quantification of the Apparent Diffusion Coefficient in Breast Lesions and its Interobserver Variability. *Diagn Interv Radiol* (2015) 21(2):123–7. doi: 10.5152/dir.2014.14217
119. Arponen O, Arponent O, Sudah M, Masarwah A, Taina M, Rautiainen S, et al. Diffusion-Weighted Imaging in 3.0 Tesla Breast MRI: Diagnostic Performance and Tumor Characterization Using Small Subregions vs. Whole Tumor Regions of Interest. *PloS One* (2015) 10(10):e0138702. doi: 10.1371/journal.pone.0138702
120. Rahbar H, Kurland BF, Olson ML, Kitsch AE, Scheel JR, Chai X, et al. Diffusion Weighted Breast MRI: A Semi-Automated Voxel Selection Technique Improves Inter-Reader Reproducibility of Apparent Diffusion Coefficient Measurements. *J Comput Assist Tomogr* (2016) 40(3):428–35. doi: 10.1097/RCT.0000000000000372
121. O'Donnell LJ, Westin C-F. An Introduction to Diffusion Tensor Image Analysis. *Neurosurg Clin N Am* (2011) 22(2):185–viii. doi: 10.1016/j.nec.2010.12.004
122. Soares J, Marques P, Alves V, Sousa N. A Hitchhiker's Guide to Diffusion Tensor Imaging. *Front Neurosci* (2013) 7:31. doi: 10.3389/fnins.2013.00031
123. Eyal E, Shapiro-Feinberg M, Furman-Haran E, Grobgeld D, Golan T, Itzchak Y, et al. Parametric Diffusion Tensor Imaging of the Breast. *Invest Radiol* (2012) 47(5):284–91. doi: 10.1097/RLI.0b013e3182438e5d
124. Jones DK, Horsfield MA, Simmons A. Optimal Strategies for Measuring Diffusion in Anisotropic Systems by Magnetic Resonance Imaging. *Magn Reson Med* (1999) 42(3):515–25. doi: 10.1002/(SICI)1522-2594(199909)42:3<515::AID-MRM14>3.0.CO;2-Q
125. Le Bihan D, Mangin JF, Poupon C, Clark CA, Pappata S, Molko N, et al. Diffusion Tensor Imaging: Concepts and Applications. *J Magn Reson Imaging* (2001) 13(4):534–46. doi: 10.1002/jmri.1076

126. Furman-Haran E, Grobgeld D, Nissan N, Shapiro-Feinberg M, Degani H. Can Diffusion Tensor Anisotropy Indices Assist in Breast Cancer Detection? *J Magn Reson Imaging* (2016) 44(6):1624–32. doi: 10.1002/jmri.25292
127. Kubicki M, Westin C-F, Maier SE, Mamata H, Frumin M, Ersner-Hershfield H, et al. Diffusion Tensor Imaging and its Application to Neuropsychiatric Disorders. *Harv Rev Psychiatry* (2002) 10(6):324–36. doi: 10.1080/10673220216231
128. Onaygil C, Kaya H, Ugurlu MU, Aribal E. Diagnostic Performance of Diffusion Tensor Imaging Parameters in Breast Cancer and Correlation With the Prognostic Factors. *J Magn Reson Imaging* (2017) 45(3):660–72. doi: 10.1002/jmri.25481
129. Wiederer J, Pazahr S, Leo C, Nanz D, Boss A. Quantitative Breast MRI: 2D Histogram Analysis of Diffusion Tensor Parameters in Normal Tissue. *Magn Reson Mater Phy* (2014) 27(2):185–93. doi: 10.1007/s10334-013-0400-9
130. Partridge SC, Murthy RS, Ziadloo A, White SW, Allison KH, Lehman CD. Diffusion Tensor Magnetic Resonance Imaging of the Normal Breast. *Magn Reson Imaging* (2010) 28(3):320–8. doi: 10.1016/j.mri.2009.10.003
131. Plaza MJ, Morris EA, Thakur SB. Diffusion Tensor Imaging in the Normal Breast: Influences of Fibroglandular Tissue Composition and Background Parenchymal Enhancement. *Clin Imaging* (2016) 40(3):506–11. doi: 10.1016/j.clinimag.2015.12.001
132. Nissan N, Furman-Haran E, Shapiro-Feinberg M, Grobgeld D, Degani H. Diffusion-Tensor MR Imaging of the Breast: Hormonal Regulation. *Radiology* (2014) 271(3):672–80. doi: 10.1148/radiol.14132084
133. Shapiro-Feinberg M, Weisenberg N, Zehavi T, Furman-Haran E, Grobgeld D, Nissan N, et al. Clinical Results of DTI. *Eur J Radiol* (2012) 81:S151–2. doi: 10.1016/S0720-048X(12)70063-3
134. Nissan N, Allweis T, Menes T, Brodsky A, Paluch-Shimon S, Haas I, et al. Breast MRI During Lactation: Effects on Tumor Conspicuity Using Dynamic Contrast-Enhanced (DCE) in Comparison With Diffusion Tensor Imaging (DTI) Parametric Maps. *Eur Radiol* (2020) 30(2):767–77. doi: 10.1007/s00330-019-06435-x
135. Partridge SC, McKinnon GC, Henry RG, Hylton NM. Menstrual Cycle Variation of Apparent Diffusion Coefficients Measured in the Normal Breast Using MRI. *J Magn Reson Imaging* (2001) 14(4):433–8. doi: 10.1002/jmri.1204
136. McDonald ES, Schopp JG, Peacock S, DeMartini WB, DeMartini WD, Rahbar H, et al. Diffusion-Weighted MRI: Association Between Patient Characteristics and Apparent Diffusion Coefficients of Normal Breast Fibroglandular Tissue at 3 T. *AJR Am J Roentgenol* (2014) 202(5):W496–502. doi: 10.2214/AJR.13.11159
137. Kim JY, Suh HB, Kang HJ, Shin JK, Choo KS, Nam KJ, et al. Apparent Diffusion Coefficient of Breast Cancer and Normal Fibroglandular Tissue in Diffusion-Weighted Imaging: The Effects of Menstrual Cycle and Menopausal Status. *Breast Cancer Res Treat* (2016) 157(1):31–40. doi: 10.1007/s10549-016-3793-0
138. Kuhl CK, Bieling HB, Gieseke J, Kreft BP, Sommer T, Lutterbey G, et al. Healthy Premenopausal Breast Parenchyma in Dynamic Contrast-Enhanced MR Imaging of the Breast: Normal Contrast Medium Enhancement and Cyclical-Phase Dependency. *Radiology* (1997) 203(1):137–44. doi: 10.1148/radiology.203.1.9122382
139. Müller-Schimpfle M, Ohmenhaüser K, Stoll P, Dietz K, Claussen CD. Menstrual Cycle and Age: Influence on Parenchymal Contrast Medium Enhancement in MR Imaging of the Breast. *Radiology* (1997) 203(1):145–9. doi: 10.1148/radiology.203.1.9122383
140. Wang K, Li Z, Wu Z, Zheng Y, Zeng S, Linning E, et al. Diagnostic Performance of Diffusion Tensor Imaging for Characterizing Breast Tumors: A Comprehensive Meta-Analysis. *Front Oncol* (2019) 9:1229. doi: 10.3389/fonc.2019.01229
141. Jiang R, Zeng X, Sun S, Ma Z, Wang X. Assessing Detection, Discrimination, and Risk of Breast Cancer According to Anisotropy Parameters of Diffusion Tensor Imaging. *Med Sci Monit* (2016) 22:1318–28. doi: 10.12659/MSM.895755
142. Kim JY, Kim JJ, Kim S, Choo KS, Kim A, Kang T, et al. Diffusion Tensor Magnetic Resonance Imaging of Breast Cancer: Associations Between Diffusion Metrics and Histological Prognostic Factors. *Eur Radiol* (2018) 28(8):3185–93. doi: 10.1007/s00330-018-5429-8
143. Ozal ST, Inci E, Gemici AA, Turgut H, Cikot M, Karabulut M. Can 3.0 Tesla Diffusion Tensor Imaging Parameters be Prognostic Indicators in Breast Cancer? *Clin Imaging* (2018) 51:240–7. doi: 10.1016/j.clinimag.2018.03.022
144. Yamaguchi K, Nakazono T, Egashira R, Komori Y, Nakamura J, Noguchi T, et al. Diagnostic Performance of Diffusion Tensor Imaging With Readout-Segmented Echo-Planar Imaging for Invasive Breast Cancer: Correlation of ADC and FA With Pathological Prognostic Markers. *Magn Reson Med Sci* (2017) 16(3):245–52. doi: 10.2463/mrms.mp.2016-0037
145. Furman-Haran E, Nissan N, Ricart-Selma V, Martinez-Rubio C, Degani H, Camps-Herrero J. Quantitative Evaluation of Breast Cancer Response to Neoadjuvant Chemotherapy by Diffusion Tensor Imaging: Initial Results. *J Magn Reson Imaging* (2018) 47(4):1080–90. doi: 10.1002/jmri.25855
146. Laun FB, Schad LR, Klein J, Stieltjes B. How Background Noise Shifts Eigenvectors and Increases Eigenvalues in DTI. *Magn Reson Mater Phy* (2009) 22(3):151–8. doi: 10.1007/s10334-008-0159-6
147. Le Bihan D, Breton E, Lallemand D, Grenier P, Cabanis E, Laval-Jeantet M. MR Imaging of Intravoxel Incoherent Motions: Application to Diffusion and Perfusion in Neurologic Disorders. *Radiology* (1986) 161(2):401–7. doi: 10.1148/radiology.161.2.3763909
148. Sigmund EE, Cho GY, Kim S, Finn M, Moccaldi M, Jensen JH, et al. Intravoxel Incoherent Motion Imaging of Tumor Microenvironment in Locally Advanced Breast Cancer: IVIM Imaging in Locally Advanced Breast Cancer. *Magn Reson Med* (2011) 65(5):1437–47. doi: 10.1002/mrm.22740
149. Kim Y, Ko K, Kim D, Min C, Kim SG, Joo J, et al. Intravoxel Incoherent Motion Diffusion-Weighted MR Imaging of Breast Cancer: Association With Histopathological Features and Subtypes. *BJR* (2016) 89(1063):20160140. doi: 10.1259/bjr.20160140
150. Iima M, Kataoka M, Kanao S, Onishi N, Kawai M, Ohashi A, et al. Intravoxel Incoherent Motion and Quantitative Non-Gaussian Diffusion MR Imaging: Evaluation of the Diagnostic and Prognostic Value of Several Markers of Malignant and Benign Breast Lesions. *Radiology* (2018) 287(2):432–41. doi: 10.1148/radiol.2017162853
151. Sigmund EE, Cho GY, Kim S, Finn M, Moccaldi M, Jensen JH, et al. Intravoxel Incoherent Motion (IVIM) Imaging of Tumor Microenvironment in Locally Advanced Breast Cancer. *Magn Reson Med* (2011) 65(5):1437–47. doi: 10.1002/mrm.22740
152. Bokacheva L, Kaplan JB, Giri DD, Patil S, Gnanasigamani M, Nyman CG, et al. Intravoxel Incoherent Motion Diffusion-Weighted MRI at 3.0 T Differentiates Malignant Breast Lesions From Benign Lesions and Breast Parenchyma. *J Magn Reson Imaging* (2014) 40(4):813–23. doi: 10.1002/jmri.24462
153. Iima M, Yano K, Kataoka M, Umehana M, Murata K, Kanao S, et al. Quantitative Non-Gaussian Diffusion and Intravoxel Incoherent Motion Magnetic Resonance Imaging: Differentiation of Malignant and Benign Breast Lesions. *Invest Radiol* (2015) 50(4):205–11. doi: 10.1097/RLI.0000000000000094
154. Liu C, Liang C, Liu Z, Zhang S, Huang B. Intravoxel Incoherent Motion (IVIM) in Evaluation of Breast Lesions: Comparison With Conventional DWI. *Eur J Radiol* (2013) 82(12):e782–9. doi: 10.1016/j.ejrad.2013.08.006
155. Liu C, Wang K, Chan Q, Liu Z, Zhang J, He H, et al. Intravoxel Incoherent Motion MR Imaging for Breast Lesions: Comparison and Correlation With Pharmacokinetic Evaluation From Dynamic Contrast-Enhanced MR Imaging. *Eur Radiol* (2017) 26(11):3888–98. doi: 10.1007/s00330-016-4241-6
156. Ma D, Lu F, Zou X, Zhang H, Li Y, Zhang L, et al. Intravoxel Incoherent Motion Diffusion-Weighted Imaging as an Adjunct to Dynamic Contrast-Enhanced MRI to Improve Accuracy of the Differential Diagnosis of Benign and Malignant Breast Lesions. *Magn Reson Imaging* (2017) 36:175–9. doi: 10.1016/j.mri.2016.10.005
157. Wang Q, Guo Y, Zhang J, Wang Z, Huang M, Zhang Y. Contribution of IVIM to Conventional Dynamic Contrast-Enhanced and Diffusion-Weighted MRI in Differentiating Benign From Malignant Breast Masses. *Breast Care (Basel)* (2016) 11(4):254–8. doi: 10.1159/000447765
158. Dijkstra H, Dorrius MD, Wielema M, Jaspers K, Pijnappel RM, Oudkerk M, et al. Semi-Automated Quantitative Intravoxel Incoherent Motion Analysis and its Implementation in Breast Diffusion-Weighted Imaging. *J Magn Reson Imaging* (2016) 43(5):1122–31. doi: 10.1002/jmri.25086

159. Lin N, Chen J, Hua J, Zhao J, Zhao J, Lu J. Intravoxel Incoherent Motion MR Imaging in Breast Cancer: Quantitative Analysis for Characterizing Lesions. *Int J Clin Exp Med* (2017) 10(1):1705–14.
160. Chen F, Chen P, Hamid Muhammed H, Zhang J. Intravoxel Incoherent Motion Diffusion for Identification of Breast Malignant and Benign Tumors Using Chemometrics. *BioMed Res Int* (2017) 2017:3845409. doi: 10.1155/2017/3845409
161. Zhao M, Fu K, Zhang L, Guo W, Wu Q, Bai X, et al. Intravoxel Incoherent Motion Magnetic Resonance Imaging for Breast Cancer: A Comparison With Benign Lesions and Evaluation of Heterogeneity in Different Tumor Regions With Prognostic Factors and Molecular Classification. *Oncol Lett* (2018) 16(4):5100–12. doi: 10.3892/ol.2018.9312
162. Mao X, Zou X, Yu N, Jiang X, Du J. Quantitative Evaluation of Intravoxel Incoherent Motion Diffusion-Weighted Imaging (IVIM) for Differential Diagnosis and Grading Prediction of Benign and Malignant Breast Lesions. *Med (Baltimore)* (2018) 97(26):e11109. doi: 10.1097/MD.0000000000011109
163. Bihan DL, Iima M, Federau C, Sigmund EE, Iima M, Federau C, et al. *Intravoxel Incoherent Motion (IVIM) MRI : Principles and Applications*. New York, USA: Jenny Stanford Publishing (2018).
164. Vidić I. *Multi-Parametric Diffusion Weighted Magnetic Resonance Imaging and Analysis in Breast Cancer*. Trondheim, Norway: Norwegian University of Science and Technology (2019).
165. Li K, Machireddy A, Tudorica A, Moloney B, Oh KY, Jafarian N, et al. Discrimination of Malignant and Benign Breast Lesions Using Quantitative Multiparametric MRI: A Preliminary Study. *Tomography* (2020) 6(2):148–59. doi: 10.18383/j.tom.2019.00028
166. Lee YJ, Kim SH, Kang BJ, Kang YJ, Yoo H, Yoo J, et al. Intravoxel Incoherent Motion (IVIM)-Derived Parameters in Diffusion-Weighted MRI: Associations With Prognostic Factors in Invasive Ductal Carcinoma: IVIM Parameters of Breast Cancer. *J Magn Reson Imaging* (2017) 45(5):1394–406. doi: 10.1002/jmri.25514
167. Kawashima H, Miyati T, Ohno N, Ohno M, Inokuchi M, Ikeda H, et al. Differentiation Between Luminal-A and Luminal-B Breast Cancer Using Intravoxel Incoherent Motion and Dynamic Contrast-Enhanced Magnetic Resonance Imaging. *Acad Radiol* (2017) 24(12):1575–81. doi: 10.1016/j.acra.2017.06.016
168. You C, Li J, Zhi W, Chen Y, Yang W, Gu Y, et al. The Volumetric-Tumour Histogram-Based Analysis of Intravoxel Incoherent Motion and non-Gaussian Diffusion MRI: Association With Prognostic Factors in HER2-Positive Breast Cancer. *J Transl Med* (2019) 17(1):182. doi: 10.1186/s12967-019-1911-6
169. Lee YJ, Kim SH, Kang BJ, Son YH, Grimm R. Associations Between Angiogenic Factors and Intravoxel Incoherent Motion-Derived Parameters in Diffusion-Weighted Magnetic Resonance Imaging of Breast Cancer. *Medicine* (2021) 100(41):e27495. doi: 10.1097/MD.0000000000027495
170. Vidić I, Egnell L, Jerome NP, Teruel JR, Sjøbakk TE, Østlie A, et al. Support Vector Machine for Breast Cancer Classification Using Diffusion-Weighted MRI Histogram Features: Preliminary Study. *J Magn Reson Imaging* (2018) 47(5):1205–16. doi: 10.1002/jmri.25873
171. Che S, Zhao X, Ou Y, Li J, Wang M, Wu B, et al. Role of the Intravoxel Incoherent Motion Diffusion Weighted Imaging in the Pre-Treatment Prediction and Early Response Monitoring to Neoadjuvant Chemotherapy in Locally Advanced Breast Cancer. *Med (Baltimore)* (2016) 95(4):e2420. doi: 10.1097/MD.0000000000002420
172. Kim Y, Kim SH, Lee HW, Song BJ, Kang BJ, Lee A, et al. Intravoxel Incoherent Motion Diffusion-Weighted MRI for Predicting Response to Neoadjuvant Chemotherapy in Breast Cancer. *Magn Reson Imaging* (2018) 48:27–33. doi: 10.1016/j.mri.2017.12.018
173. Cho GY, Gennaro L, Sutton EJ, Zabor EC, Zhang Z, Giri D, et al. Intravoxel Incoherent Motion (IVIM) Histogram Biomarkers for Prediction of Neoadjuvant Treatment Response in Breast Cancer Patients. *Eur J Radiol Open* (2017) 4:101–7. doi: 10.1016/j.ejro.2017.07.002
174. Cho GY, Moy L, Zhang JL, Baete S, Lattanzi R, Moccaldi M, et al. Comparison of Fitting Methods and B-Value Sampling Strategies for Intravoxel Incoherent Motion in Breast Cancer. *Magn Reson Med* (2015) 74(4):1077–85. doi: 10.1002/mrm.25484
175. Suo S, Lin N, Wang H, Zhang L, Wang R, Zhang S, et al. Intravoxel Incoherent Motion Diffusion-Weighted MR Imaging of Breast Cancer at 3.0 Tesla: Comparison of Different Curve-Fitting Methods. *J Magn Reson Imaging* (2015) 42(2):362–70. doi: 10.1002/jmri.24799
176. Chen W, Zhang J, Long D, Wang Z, Zhu J. Optimization of Intra-Voxel Incoherent Motion Measurement in Diffusion-Weighted Imaging of Breast Cancer. *J Appl Clin Med Phys* (2017) 18(3):191–9. doi: 10.1002/acm2.12065
177. While PT. A Comparative Simulation Study of Bayesian Fitting Approaches to Intravoxel Incoherent Motion Modeling in Diffusion-Weighted MRI. *Magn Reson Med* (2017) 78(6):2373–87. doi: 10.1002/mrm.26598
178. Vidić I, Jerome NP, Bathen TF, Goa PE, While PT. Accuracy of Breast Cancer Lesion Classification Using Intravoxel Incoherent Motion Diffusion-Weighted Imaging is Improved by the Inclusion of Global or Local Prior Knowledge With Bayesian Methods. *J Magn Reson Imaging* (2019) 50(5):1478–88. doi: 10.1002/jmri.26772
179. While PT, Teruel JR, Vidić I, Bathen TF, Goa PE. Relative Enhanced Diffusivity: Noise Sensitivity, Protocol Optimization, and the Relation to Intravoxel Incoherent Motion. *Magn Reson Mater Phy* (2018) 31(3):425–38. doi: 10.1007/s10334-017-0660-x
180. Teruel JR, Goa PE, Sjøbakk TE, Østlie A, Fjøsne HE, Bathen TF. A Simplified Approach to Measure the Effect of the Microvasculature in Diffusion-Weighted MR Imaging Applied to Breast Tumors: Preliminary Results. *Radiology* (2016) 281(2):373–81. doi: 10.1148/radiol.2016151630
181. Jensen JH, Helpern JA, Ramani A, Lu H, Kaczynski K. Diffusional Kurtosis Imaging: The Quantification of non-Gaussian Water Diffusion by Means of Magnetic Resonance Imaging. *Magn Reson Med* (2005) 53(6):1432–40. doi: 10.1002/mrm.20508
182. Wu D, Li G, Zhang J, Chang S, Hu J, Dai Y. Characterization of Breast Tumors Using Diffusion Kurtosis Imaging (DKI). *PloS One* (2014) 9(11):e113240. doi: 10.1371/journal.pone.0113240
183. Christou A, Ghiatas A, Priovolos D, Veliou K, Bougias H. Accuracy of Diffusion Kurtosis Imaging in Characterization of Breast Lesions. *Br J Radiol* (2017) 90(1073):20160873. doi: 10.1259/bjr.20160873
184. Nogueira L, Brandão S, Matos E, Nunes RG, Loureiro J, Ramos I, et al. Application of the Diffusion Kurtosis Model for the Study of Breast Lesions. *Eur Radiol* (2014) 24(6):1197–203. doi: 10.1007/s00330-014-3146-5
185. Liu W, Wei C, Bai J, Gao X, Zhou L. Histogram Analysis of Diffusion Kurtosis Imaging in the Differentiation of Malignant From Benign Breast Lesions. *Eur J Radiol* (2019) 117:156–63. doi: 10.1016/j.ejrad.2019.06.008
186. Meng N, Wang X, Sun J, Han D, Bai Y, Wei W, et al. A Comparative Study of the Value of Amide Proton Transfer-Weighted Imaging and Diffusion Kurtosis Imaging in the Diagnosis and Evaluation of Breast Cancer. *Eur Radiol* (2021) 31(3):1707–17. doi: 10.1007/s00330-020-07169-x
187. Sun K, Chen X, Chai W, Fei X, Fu C, Yan X, et al. Breast Cancer: Diffusion Kurtosis MR Imaging—Diagnostic Accuracy and Correlation With Clinical-Pathologic Factors. *Radiology* (2015) 277(1):46–55. doi: 10.1148/radiol.15141625
188. Zhou W-P, Zan X-Y, Hu X-Y, Liu X, Sudarshan SKP, Yang S-D, et al. Characterization of Breast Lesions Using Diffusion Kurtosis Model-Based Imaging: An Initial Experience. *J Xray Sci Technol* (2020) 28(1):157–69. doi: 10.3233/XST-190590
189. Li T, Hong Y, Kong D, Li K. Histogram Analysis of Diffusion Kurtosis Imaging Based on Whole-Volume Images of Breast Lesions. *J Magn Reson Imaging* (2020) 51(2):627–34. doi: 10.1002/jmri.26884
190. Huang Y, Lin Y, Hu W, Ma C, Lin W, Wang Z, et al. Diffusion Kurtosis at 3.0T as an *In Vivo* Imaging Marker for Breast Cancer Characterization: Correlation With Prognostic Factors. *J Magn Reson Imaging* (2019) 49(3):845–56. doi: 10.1002/jmri.26249
191. Palm T, Wenkel E, Ohlmeyer S, Janka R, Uder M, Weiland E, et al. Diffusion Kurtosis Imaging Does Not Improve Differentiation Performance of Breast Lesions in a Short Clinical Protocol. *Magn Reson Imaging* (2019) 63:205–16. doi: 10.1016/j.mri.2019.08.007
192. Wu J, Yan F, Chai W, Fu C, Yan X, Zhan Y, et al. Breast Cancer Recurrence Risk Prediction Using Whole-Lesion Histogram Analysis With Diffusion Kurtosis Imaging. *Clin Radiol* (2020) 75(3):239.e1–8. doi: 10.1016/j.crad.2019.10.015
193. Mlynarska-Bujny A, Bickelhaupt S, Laun FB, König F, Lederer W, Daniel H, et al. Influence of Residual Fat Signal on Diffusion Kurtosis MRI of Suspicious Mammography Findings. *Sci Rep* (2020) 10(1):13286. doi: 10.1038/s41598-020-70154-3

194. Iima M, Honda M, Sigmund EE, Ohno Kishimoto A, Kataoka M, Togashi K. Diffusion MRI of the Breast: Current Status and Future Directions. *J Magn Reson Imaging* (2020) 52(1):70–90. doi: 10.1002/jmri.26908
195. Choi BH, Baek HJ, Ha JY, Ryu KH, Moon JI, Park SE, et al. Feasibility Study of Synthetic Diffusion-Weighted MRI in Patients With Breast Cancer in Comparison With Conventional Diffusion-Weighted MRI. *Korean J Radiol* (2020) 21(9):1036–44. doi: 10.3348/kjr.2019.0568
196. Bickel H, Polanec SH, Wengert G, Pinker K, Bogner W, Helbich TH, et al. Diffusion-Weighted MRI of Breast Cancer: Improved Lesion Visibility and Image Quality Using Synthetic B-Values. *J Magn Reson Imaging* (2019) 50 (6):1754–61. doi: 10.1002/jmri.26809
197. Jin Y-N, Zhang Y, Cheng J-L, Zheng D-D, Hu Y. Monoexponential, Biexponential, and Stretched-Exponential Models Using Diffusion-Weighted Imaging: A Quantitative Differentiation of Breast Lesions at 3.0T. *J Magn Reson Imaging* (2019) 50(5):1461–7. doi: 10.1002/jmri.26729
198. Ertas G, Onaygil C, Akin Y, Kaya H, Aribal E. Quantitative Differentiation of Breast Lesions at 3T Diffusion-Weighted Imaging (DWI) Using the Ratio of Distributed Diffusion Coefficient (DDC). *J Magn Reson Imaging* (2016) 44 (6):1633–41. doi: 10.1002/jmri.25327
199. Liu C, Wang K, Li X, Zhang J, Ding J, Spuhler K, et al. Breast Lesion Characterization Using Whole-Lesion Histogram Analysis With Stretched-Exponential Diffusion Model. *J Magn Reson Imaging* (2018) 47(6):1701–10. doi: 10.1002/jmri.25904
200. Chen B-Y, Xie Z, Nie P, Yang D, Hu Y-C, Liu S-T, et al. Multiple B-Value Diffusion-Weighted Imaging in Differentiating Benign From Malignant Breast Lesions: Comparison of Conventional Mono-, Bi- and Stretched Exponential Models. *Clin Radiol* (2020) 75(8):642.e1–8. doi: 10.1016/j.crad.2020.03.039
201. Goto M, Le Bihan D, Yoshida M, Sakai K, Yamada K. Adding a Model-Free Diffusion MRI Marker to BI-RADS Assessment Improves Specificity for Diagnosing Breast Lesions. *Radiology* (2019) 292(1):84–93. doi: 10.1148/radiol.2019181780
202. Brunsing RL, Schenker-Ahmed NM, White NS, Parsons JK, Kane C, Kuperman J, et al. Restriction Spectrum Imaging: An Evolving Imaging Biomarker in Prostate MRI. *J Magn Reson Imaging* (2017) 45(2):323–36. doi: 10.1002/jmri.25419
203. White NS, Leergaard TB, D'Arceuil H, Bjaalie JG, Dale AM. Probing Tissue Microstructure With Restriction Spectrum Imaging: Histological and Theoretical Validation. *Hum Brain Mapp* (2013) 34(2):327–46. doi: 10.1002/hbm.21454
204. White NS, Dale AM. Distinct Effects of Nuclear Volume Fraction and Cell Diameter on High B-Value Diffusion MRI Contrast in Tumors. *Magn Reson Med* (2014) 72(5):1435–43. doi: 10.1002/mrm.25039
205. Rodríguez-Soto AE, Andreassen MMS, Fang LK, Conlin CC, Park HH, Ahn GS, et al. Characterization of the Diffusion Signal of Breast Tissues Using Multi-Exponential Models. *Magn Reson Med* (2022) 87(4):1938–51. doi: 10.1101/2020.04.27.20082271
206. Andreassen MMS, Rodríguez-Soto AE, Conlin CC, Vidić I, Seibert TM, Wallace AM, et al. Discrimination of Breast Cancer From Healthy Breast Tissue Using a Three-Component Diffusion-Weighted MRI Model. *Clin Cancer Res* (2021) 27(4):1094–104. doi: 10.1158/1078-0432.CCR-20-2017
207. Rodríguez-Soto AE, Meriwether CH, Park AJ, Adams DWJR, Wallace A, Ojeda-Fournier H, et al. Noncontrast MRI With Advanced Diffusion Weighted Imaging for Breast Cancer Detection in a Lactating Woman. *Radiol Case Rep* (2020) 15(11):2358–61. doi: 10.1016/j.radcr.2020.08.058
208. Dialani V. *Comparing Restriction Spectrum Imaging (RSI) to Conventional and Abbreviated Breast MRI for Breast Cancer Screening* (2021). Available at: https://clinicaltrials.gov/ct2/show/NCT03495115.
209. Reynaud O. Time-Dependent Diffusion MRI in Cancer: Tissue Modeling and Applications. *Front Phys* (2017) 5. doi: 10.3389/fphy.2017.00058
210. Iima M, Nobashi T, Imai H, Koyasu S, Saga T, Nakamoto Y, et al. Effects of Diffusion Time on non-Gaussian Diffusion and Intravoxel Incoherent Motion (IVIM) MRI Parameters in Breast Cancer and Hepatocellular Carcinoma Xenograft Models. *Acta Radiol Open* (2018) 7(1):2058460117751565. doi: 10.1177/2058460117751565
211. Jiang X, Li H, Xie J, Zhao P, Gore JC, Xu J. Quantification of Cell Size Using Temporal Diffusion Spectroscopy. *Magn Reson Med* (2016) 75(3):1076–85. doi: 10.1002/mrm.25684
212. Teruel JR, Cho GY, Rt MM, Goa PE, Bathen TF, Feiweier T, et al. Stimulated Echo Diffusion Tensor Imaging (STEAM-DTI) With Varying Diffusion Times as a Probe of Breast Tissue. *J Magn Reson Imaging* (2017) 45(1):84–93. doi: 10.1002/jmri.25376
213. Colvin DC, Loveless ME, Does MD, Yue Z, Yankeelov TE, Gore JC. Earlier Detection of Tumor Treatment Response Using Magnetic Resonance Diffusion Imaging With Oscillating Gradients. *Magn Reson Imaging* (2011) 29(3):315–23. doi: 10.1016/j.mri.2010.10.003
214. Xu J, Jiang X, Li H, Arlinghaus LR, McKinley ET, Devan SP, et al. Magnetic Resonance Imaging of Mean Cell Size in Human Breast Tumors. *arXiv* (2020) 83(6):2002–14. doi: 10.1002/mrm.28056
215. Gore JC, Xu J, Colvin DC, Yankeelov TE, Parsons EC, Does MD. Characterization of Tissue Structure at Varying Length Scales Using Temporal Diffusion Spectroscopy. *NMR BioMed* (2010) 23(7):745–56. doi: 10.1002/nbm.1531
216. Ye D-M, Wang H-T, Yu T. The Application of Radiomics in Breast MRI: A Review. *Technol Cancer Res Treat* (2020) 19:1533033820916191. doi: 10.1177/1533033820916191
217. Kumar V, Gu Y, Basu S, Berglund A, Eschrich SA, Schabath MB, et al. Radiomics: The Process and the Challenges. *Magn Reson Imaging* (2012) 30 (9):1234–48. doi: 10.1016/j.mri.2012.06.010
218. Bickelhaupt S, Jaeger PF, Laun FB, Lederer W, Daniel H, Kuder TA, et al. Radiomics Based on Adapted Diffusion Kurtosis Imaging Helps to Clarify Most Mammographic Findings Suspicious for Cancer. *Radiology* (2018) 287 (3):761–70. doi: 10.1148/radiol.2017170273
219. Bickelhaupt S, Paech D, Kickingereder P, Steudle F, Lederer W, Daniel H, et al. Prediction of Malignancy by a Radiomic Signature From Contrast Agent-Free Diffusion MRI in Suspicious Breast Lesions Found on Screening Mammography. *J Magn Reson Imaging* (2017) 46(2):604–16. doi: 10.1002/jmri.25606
220. Jiang X, Xie F, Liu L, Peng Y, Cai H, Li L. Discrimination of Malignant and Benign Breast Masses Using Automatic Segmentation and Features Extracted From Dynamic Contrast-Enhanced and Diffusion-Weighted MRI. *Oncol Lett* (2018) 16(2):1521–8. doi: 10.3892/ol.2018.8805
221. Zhang Q, Peng Y, Liu W, Bai J, Zheng J, Yang X, et al. Radiomics Based on Multimodal MRI for the Differential Diagnosis of Benign and Malignant Breast Lesions. *J Magn Reson Imaging* (2020) 52(2):596–607. doi: 10.1002/jmri.27098
222. Parekh VS, Jacobs MA. Integrated Radiomic Framework for Breast Cancer and Tumor Biology Using Advanced Machine Learning and Multiparametric MRI. *NPJ Breast Cancer* (2017) 3:43. doi: 10.1038/s41523-017-0045-3
223. Holli-Helenius K, Salminen A, Rinta-Kiikka I, Koskivuo I, Brück N, Boström P, et al. MRI Texture Analysis in Differentiating Luminal A and Luminal B Breast Cancer Molecular Subtypes - a Feasibility Study. *BMC Med Imaging* (2017) 17(1):69. doi: 10.1186/s12880-017-0239-z
224. Sun X, He B, Luo X, Li Y, Cao J, Wang J, et al. Preliminary Study on Molecular Subtypes of Breast Cancer Based on Magnetic Resonance Imaging Texture Analysis. *J Comput Assisted Tomogr* (2018) 42(4):531–5. doi: 10.1097/RCT.0000000000000738
225. Xie T, Wang Z, Zhao Q, Bai Q, Zhou X, Gu Y, et al. Machine Learning-Based Analysis of MR Multiparametric Radiomics for the Subtype Classification of Breast Cancer. *Front Oncol* (2019) 9:505. doi: 10.3389/fonc.2019.00505
226. Xie T, Zhao Q, Fu C, Bai Q, Zhou X, Li L, et al. Differentiation of Triple-Negative Breast Cancer From Other Subtypes Through Whole-Tumor Histogram Analysis on Multiparametric MR Imaging. *Eur Radiol* (2019) 29(5):2535–44. doi: 10.1007/s00330-018-5804-5
227. Leithner D, Bernard-Davila B, Martinez DF, Horvat JV, Jochelson MS, Marino MA, et al. Radiomic Signatures Derived From Diffusion-Weighted Imaging for the Assessment of Breast Cancer Receptor Status and Molecular Subtypes. *Mol Imaging Biol* (2020) 22(2):453–61. doi: 10.1007/s11307-019-01383-w
228. Dong Y, Feng Q, Yang W, Lu Z, Deng C, Zhang L, et al. Preoperative Prediction of Sentinel Lymph Node Metastasis in Breast Cancer Based on Radiomics of T2-Weighted Fat-Suppression and Diffusion-Weighted MRI. *Eur Radiol* (2018) 28(2):582–91. doi: 10.1007/s00330-017-5005-7
229. Chai R, Ma H, Xu M, Arefan D, Cui X, Liu Y, et al. Differentiating Axillary Lymph Node Metastasis in Invasive Breast Cancer Patients: A Comparison

of Radiomic Signatures From Multiparametric Breast MR Sequences. *J Magn Reson Imaging* (2019) 50(4):1125–32. doi: 10.1002/jmri.26701
230. Liu W, Cheng Y, Liu Z, Liu C, Cattell R, Xie X, et al. Preoperative Prediction of Ki-67 Status in Breast Cancer With Multiparametric MRI Using Transfer Learning. *Acad Radiol* (2021) 28(2):e44–53. doi: 10.1016/j.acra.2020.02.006
231. Zhang Y, Zhu Y, Zhang K, Liu Y, Cui J, Tao J, et al. Invasive Ductal Breast Cancer: Preoperative Predict Ki-67 Index Based on Radiomics of ADC Maps. *La radiologia media* (2019) 125(2):109–16. doi: 10.1007/s11547-019-01100-1
232. Fan M, Yuan W, Zhao W, Xu M, Wang S, Gao X, et al. Joint Prediction of Breast Cancer Histological Grade and Ki-67 Expression Level Based on DCE-MRI and DWI Radiomics. *IEEE J Biomed Health Inf* (2020) 24 (6):1632–42. doi: 10.1109/JBHI.2019.2956351
233. Fan M, Liu Z, Xu M, Wang S, Zeng T, Gao X, et al. Generative Adversarial Network-Based Super-Resolution of Diffusion-Weighted Imaging: Application to Tumour Radiomics in Breast Cancer. *NMR Biomed* (2020) 33(8):e4345. doi: 10.1002/nbm.4345
234. Liu Z, Li Z, Qu J, Zhang R, Zhou X, Li L, et al. Radiomics of Multiparametric MRI for Pretreatment Prediction of Pathologic Complete Response to Neoadjuvant Chemotherapy in Breast Cancer: A Multicenter Study. *Clin Cancer Res* (2019) 25(12):3538–47. doi: 10.1158/1078-0432.CCR-18-3190
235. Michoux N, Van den Broeck S, Lacoste L, Fellah L, Galant C, Berlière M, et al. Texture Analysis on MR Images Helps Predicting non-Response to NAC in Breast Cancer. *BMC Cancer* (2015) 15:574. doi: 10.1186/s12885-015-1563-8
236. Panzeri MM, Losio C, Della Corte A, Venturini E, Ambrosi A, Panizza P, et al. Prediction of Chemoresistance in Women Undergoing Neo-Adjuvant Chemotherapy for Locally Advanced Breast Cancer: Volumetric Analysis of First-Order Textural Features Extracted From Multiparametric MRI. *Contrast Media Mol Imaging* (2018) 2018:1–7. doi: 10.1155/2018/8329041
237. Schmitz AMT, Veldhuis WB, Menke-Pluijmers MBE, van der Kemp WJM, van der Velden TA, Kock MCJM, et al. Multiparametric MRI With Dynamic Contrast Enhancement, Diffusion-Weighted Imaging, and 31-Phosphorus Spectroscopy at 7 T for Characterization of Breast Cancer. *Invest Radiol* (2015) 50(11):766–71. doi: 10.1097/RLI.0000000000000183
238. Bogner W, Pinker K, Zaric O, Baltzer P, Minarikova L, Porter D, et al. Bilateral Diffusion-Weighted MR Imaging of Breast Tumors With Submillimeter Resolution Using Readout-Segmented Echo-Planar Imaging at 7 T. *Radiology* (2014) 274(1):74–84. doi: 10.1148/radiol.14132340
239. Gruber S, Minarikova L, Pinker K, Zaric O, Chmelik M, Strasser B, et al. Diffusion-Weighted Imaging of Breast Tumours at 3 Tesla and 7 Tesla: A Comparison. *Eur Radiol* (2016) 26(5):1466–73. doi: 10.1007/s00330-015-3947-1
240. Korteweg MA, Veldhuis WB, Visser F, Luijten PR, Mali WPTM, van Diest PJ, et al. Feasibility of 7 Tesla Breast Magnetic Resonance Imaging Determination of Intrinsic Sensitivity and High-Resolution Magnetic Resonance Imaging, Diffusion-Weighted Imaging, and (1)H-Magnetic Resonance Spectroscopy of Breast Cancer Patients Receiving Neoadjuvant Therapy. *Invest Radiol* (2011) 46 (6):370–6. doi: 10.1097/RLI.0b013e31820df706
241. Iima M, Le Bihan D. Clinical Intravoxel Incoherent Motion and Diffusion MR Imaging: Past, Present, and Future. *Radiology* (2015) 278(1):13–32. doi: 10.1148/radiol.2015150244

Conflict of Interest: RR-P: Human Longevity Inc: Consultant, Cortech Labs: Stock options, Curemetrix: Stock options, consultant. and GE: research agreement.

The remaining authors declare that the research was conducted in the absence of any commercial or financial relationships that could be construed as a potential conflict of interest.